



HAL
open science

A MICROMECHANICS-BASED CLASSIFICATION OF THE REGIMES DELINEATING THE BEHAVIOUR OF GAP-GRADED SOILS

Peter Adesina, Antoine Wautier, Nadia Benahmed

► **To cite this version:**

Peter Adesina, Antoine Wautier, Nadia Benahmed. A MICROMECHANICS-BASED CLASSIFICATION OF THE REGIMES DELINEATING THE BEHAVIOUR OF GAP-GRADED SOILS. Computers and Geotechnics, 2024, 168, pp.106165. 10.1016/j.compgeo.2024.106165 . hal-04464980

HAL Id: hal-04464980

<https://hal.inrae.fr/hal-04464980v1>

Submitted on 19 Feb 2024

HAL is a multi-disciplinary open access archive for the deposit and dissemination of scientific research documents, whether they are published or not. The documents may come from teaching and research institutions in France or abroad, or from public or private research centers.

L'archive ouverte pluridisciplinaire **HAL**, est destinée au dépôt et à la diffusion de documents scientifiques de niveau recherche, publiés ou non, émanant des établissements d'enseignement et de recherche français ou étrangers, des laboratoires publics ou privés.



Distributed under a Creative Commons Attribution 4.0 International License

A MICROMECHANICS-BASED CLASSIFICATION OF THE REGIMES DELINEATING THE BEHAVIOUR OF GAP-GRADED SOILS

Peter Adesina^{1*}, Antoine Wautier², Nadia Benahmed³

^{1,2,3}INRAE, Aix-Marseille University; UMR RECOVER, 3275 Rte Cézanne, CS 40061, 13182
Aix-en-Provence, France

*Corresponding author. E-mail addresses: peter.adesina@inrae.fr, greatpetson121@gmail.com
(P. Adesina); antoine.wautier@inrae.fr (Antoine Wautier); nadia.benahmed@inrae.fr (Nadia Benahmed)

Abstract

This study presents a micromechanical evaluation of the regimes delineating the behaviour of gap-graded granular assemblies, using discrete element simulations. Dense and loose bimodal assemblies of different fines content were prepared and subjected to drained triaxial compression until the critical state was reached. The regimes delineating the behaviour of the assemblies were evaluated, characterised and their significance discussed. While two regimes demarcated by the threshold fines content were identified based on the analysis of the macroscale characteristics of the assemblies, up to four regimes were identified based on the contributions of the particle size fractions and contact types to the total mean stress. Contrary to previous studies according to which fines control the mechanical behaviour of gap-graded assemblies from the threshold fines content, f_c^{th} , we found that the fines do not play a primary role in stress transmission until beyond a significantly larger fines content, f_c^{eq} (the equivalent fines content), which depends on density and stress state. Based on the correlation found between the critical state strength and the stress-based skeleton void ratio proposed in this study, we conclude that stress-based skeleton void ratio can be useful in understanding the mechanical response of gap-graded materials at the critical state.

Keywords: Gap-graded assemblies, regimes, density, triaxial compression, DEM

¹Post doctoral researcher, INRAE, Aix-Marseille University; UMR RECOVER, 3275 Rte Cézanne, CS 40061, 13182 Aix-en-Provence, France. Email: peter.adesina@inrae.fr; greatpetson121@gmail.com

²Research Fellow, INRAE, Aix-Marseille University; UMR RECOVER, 3275 Rte Cézanne, CS 40061, 13182 Aix-en-Provence, France. Email: antoine.wautier@inrae.fr

³Research Fellow, INRAE, Aix-Marseille University; UMR RECOVER, 3275 Rte Cézanne, CS 40061, 13182 Aix-en-Provence, France. Email: nadia.benahmed@inrae.fr

31 **1. Introduction**

32 Soil mixtures containing a coarser and a finer fraction (as in silty sands, sandy gravels, etc.)
33 are abundant in nature. It is well established that the mechanical behaviour of these mixtures
34 depends on the proportions of the coarser and the finer fraction within the mixtures. However,
35 there is no consensus in the literature on specific fine contents delineating different behaviour
36 for gap-graded granular mixtures. For example, as a result of the conceptual analysis presented
37 in experimental studies, it has been suggested that the fines play a primary role in the shear
38 behaviour of gap-graded assemblies beyond a threshold fines content (Thevanayagam et al.,
39 2002); and control the behaviour beyond a limiting fines content (Lade & Yamamuro, 1997;
40 Salgado et al., 2000; Skempton & Brogan, 1994; Vallejo, 2001). The threshold fines content is
41 usually related to geometric properties, and in particular the measure of the minimum void ratio
42 (Cubrinovski & Ishihara, 2002; Yang et al., 2005; Zuo & Baudet, 2015). From the threshold
43 fines content, the fines start to disperse the coarse particles. The limiting fines content
44 corresponds to the situation where the fines completely disperse the coarse particles (floating
45 grains in a fine matrix) (Skempton & Brogan, 1994; Thevanayagam et al., 2002). Since
46 quantifying the stress or the dispersion of individual particles within a matrix is difficult in
47 experiments, it is almost impossible to ascertain the delineating fines content of the conceptual
48 models without the use of a micromechanical framework.

49 In this regard, the discrete element method (DEM) proposed by (Cundall & Strack, 1979) has
50 been found an effective numerical tool for probing the micromechanics of granular materials.
51 DEM offers the opportunity to evaluate the assertions from the conceptual models in earlier
52 experimental studies where the stress transmitted by individual particles cannot be determined.
53 In the earlier studies where DEM has been used to assess the behaviour of gap-graded
54 assemblies, the approach adopted involved determining the proportion of the stress transmitted
55 by each particle size fraction and contact types. However, no consensus has been reached on
56 the specific fines content delineating different behaviour; in fact, the existence of some of the
57 specific fines contents suggested by experimental studies is sometimes questioned (as in Sufian
58 et al., (2021)) or not identified.

59 In this study, we conducted four analyses organised into four sections to evaluate the regimes⁴
60 delineating the behaviour of gap-graded sand-silt mixtures. In Section 3, we determined the
61 macroscale and micromechanical behaviour of the assemblies of sand-silt mixtures with fines

⁴ The word “regime” in this paper refers to zones of unique behaviour within the range of fines content in gap-graded assemblies.

62 content, f_c , within $10\% \leq f_c \leq 70\%$; and assessed the existence of regimes delineating the
63 characteristics of the assemblies. The macroscale characteristics considered are the void ratio,
64 strength and dilatancy, while the micromechanical characteristic considered is the coordination
65 number. We then conducted in Section 4, a particle-scale analysis of the contribution of the
66 finer and the coarser fractions to the total mean stress transmitted by an assembly. This enabled
67 a particle stress-based evaluation of the regimes delineating the behaviour of the assemblies.
68 Following this, in Section 5, we conducted a contact-scale analysis of the contribution of each
69 contact type to the total mean stress, again to identify existing regimes. Finally, in Section 6,
70 we present a stress-based skeleton void ratio as an alternative void ratio index to interpret the
71 strength properties of the granular mixtures studied. We assessed the performance of alternative
72 void ratio indexes such as the mechanical and the void ratio (global), in interpreting the strength
73 exhibited by the granular mixtures studied, at both the peak and the critical state. An assessment
74 of the internal instability of the gap-graded assemblies (i.e. their susceptibility to internal
75 erosion) is beyond the scope of this study. However, the implications of the findings with
76 respect to internal erosion are discussed in the conclusion.

77

78 **2. Numerical Simulation approach**

79 The DEM simulations in this study were conducted using the open-source code YADE
80 (Šmilauer et al, 2021). All assemblies were generated to have a bimodal grading of fine
81 particles with diameter, $D_f=0.375$ mm and coarse particles with diameter $D_c=3.075$ mm such
82 that the size ratio, $\lambda = D_c/D_f = 8.2$. The bimodal grading is considered the simplest type of gap-
83 graded material and was employed in this study to ensure the results obtained are solely from
84 the interaction between the coarser and the finer fractions without the interference of the
85 grading effect from within either of the fractions. The size ratio value was selected sufficiently
86 large to allow for fine migration in the pore space (should water flow be considered) (Lade et
87 al., 1998; Rahman et al., 2008; Shire et al., 2016; Thevanayagam et al., 2002).

88 After a parametric study to determine the representative element volume (REV), each assembly
89 contains 100,000 particles (Fig.1). Increasing the sample size to 200,000 particles for the $f_c =$
90 30% case at both the dense and loose states did not significantly influence the stress-strain
91 responses (see Appendix A). The slight sensitivity to sample size observed in the volumetric
92 strains was also reported in the DEM study on REV for granular materials by Adesina et al.,
93 (2022) and can be attributed to the small variation in the initial void ratio of the assemblies.

94 Table 2 shows the number of the fines and the coarse particles for each percentage of fines
95 content, f_c (%).

96 The assemblies studied here were prepared by subjecting them to isotropic compression at 100
97 kPa within six frictionless walls. The standard linear elasto-plastic model was employed to
98 simulate the interactions between particles. Table 1 shows the simulation parameters employed
99 in the simulations. Following Jiang et al., (2018), the material density in the simulations was
100 scaled to 1000 times the original value in order to increase the critical time step, $\Delta t_{cr} \propto$
101 $r\sqrt{\rho/E}$, where r is the particle radius, ρ is the density and E is the Young's modulus. A fraction
102 ($0.9\Delta t_{cr}$) of this critical time step was then applied to ensure numerical stability. While this
103 density scaling approach was adopted for computational efficiency, it does not compromise the
104 quasi-static conditions of the simulations as long as the inertial number remains sufficiently
105 small (Thornton, 2000; Thornton & Anthony, 1998). Based on the standard practice adopted in
106 prior DEM studies including (Thornton, 2000) for assembly preparation, here, assemblies of
107 different initial densities were generated by using a friction coefficient $\mu=0.03$ for the dense
108 assemblies and $\mu=0.5$ for the loose assemblies, during isotropic compression. The void ratio of
109 the dense assemblies is denoted e_{min} , while the void ratio of the loose assemblies is denoted
110 as e_{max} . It is important to note that these e_{min} and e_{max} values cannot be directly mapped to
111 the values obtained using standard procedures employed in experiments.

112 After isotropic compression, the assemblies were subjected to triaxial compression under a
113 constant confining pressure of $\sigma_{xx}=\sigma_{yy}=100$ kPa⁵ in both the x -direction and y -direction and
114 a strain rate of 0.01 s⁻¹ in the z -direction. A numerical damping coefficient of 0.05 is used.
115 These conditions ensured that for our simulations, the inertial number for the coarse particles,
116 $I_{dmax} = 1.60 \times 10^{-4}$, and that for the fines, $I_{dmin} = 1.95 \times 10^{-5}$, therefore the simulations were
117 deemed quasi-static (da Cruz et al., 2005). Prior to shearing, additional number of cycles at
118 $\mu=0.5$ was applied to equilibrate the assemblies. Also, the unbalanced force ratio⁶ was checked
119 to remain below a limit of 0.01 to guarantee static equilibrium. All assemblies were sheared at
120 $\mu=0.5$ regardless of the friction coefficient used during the assembly preparation stage. A total
121 of 22 shearing simulations were conducted in this study (11 fines contents are considered for 2
122 relative densities) (Table 2).

123
124

⁵ Throughout this paper, soil mechanics conventions are used with compression being positive and extension being negative.

⁶ The maximum resultant force on the different grains divided by the mean contact force.

125 **Table 1** Simulation parameters

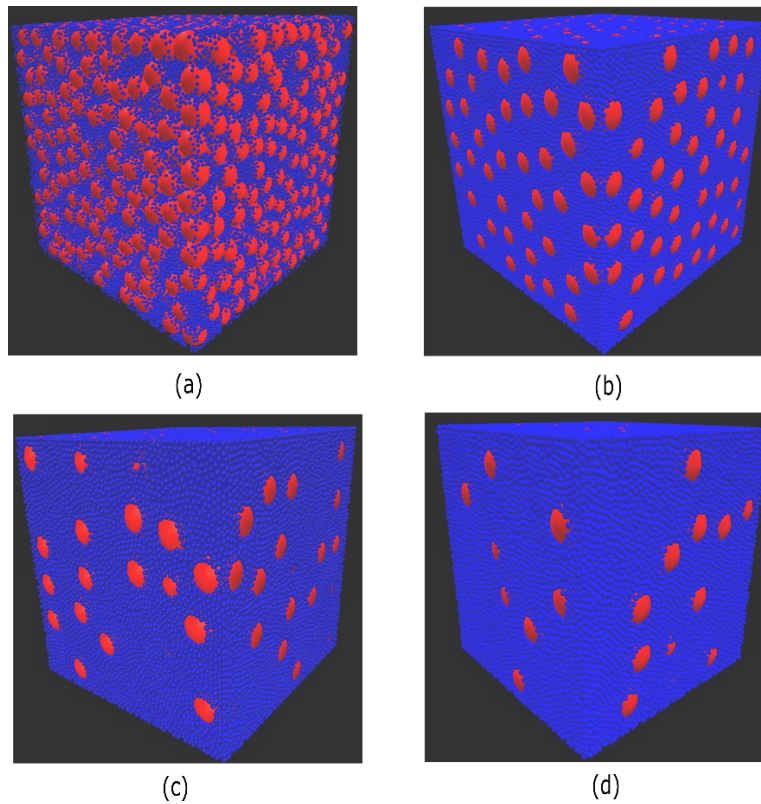
Parameter	Value
Diameter of coarse particles, D_c , mm	3.075
Diameter of fine particles, D_f , mm	0.375
Particle size ratio D_c / D_f	8.2
Particle density, ρ , kg/m^3	2700×10^3
Contact law	Elasto-frictional
Inter-particle friction coefficient during isotropic compression	0.03 (dense), 0.5 (loose)
Inter-particle friction coefficient during shearing	0.5
Wall-particle friction coefficient	0
Particle normal stiffness, k_n , N/m^2	3.56×10^8
Stiffness ratio	1.0

126

127 **Table 2** Number of particles for each assembly

Specimens		Percentage of fine particles by weight										
		10%	15%	20%	25%	30%	35%	40%	45%	50%	60%	70%
Number of particles	Coarse	1,612	1,021	723	543	423	337	272	222	182	121	78
	Fine	98,388	98,979	99,277	99,457	99,577	99,663	99,728	99,778	99,818	99,879	99,922
	Total	100,000										

128



129

130 **Fig. 1.** Dense specimens with different percentages of fines content: (a) $f_c = 10\%$ (b) $f_c = 30\%$
 131 $f_c = 50\%$ (d) $f_c = 70\%$

132

133 **3. Macro-scale and micromechanical characteristics of the binary mixtures for varying**
134 **fines content.**

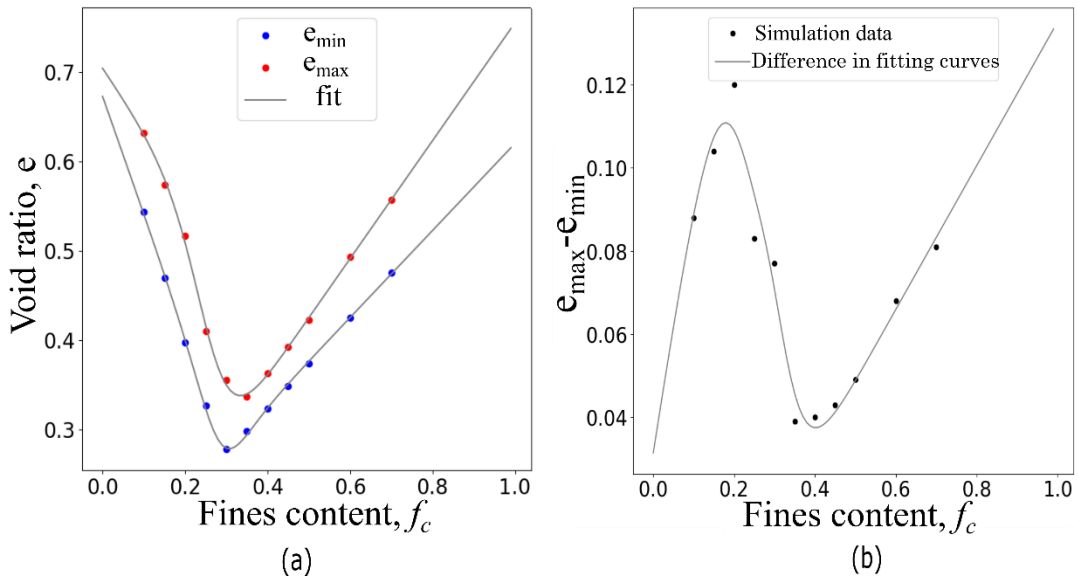
135 The initial void ratios of the gap-graded assemblies with different fines content are plotted in
136 Fig. 2a. As earlier mentioned, the void ratio of the dense and loose assemblies studied are
137 denoted as e_{min} and e_{max} , respectively. In both the dense and the loose assemblies, two regimes
138 of distinct trends are observed. The first regime is characterised by a reduction in the void ratio
139 as f_c increases. This is as a result of the fines progressively filling the voids within the coarse
140 particles. At a certain fines content referred to as the critical fines content (Skempton & Brogan,
141 1994), the threshold fines content, f_c^{th} (Lade et al., 1998; Thevanayagam et al., 2002), or the
142 transitional fines content (Yang et al., 2005), the voids within the coarse particles are fully filled
143 by the fines. The second regime corresponds to $f_c > f_c^{th}$ and it is characterised by an increase in
144 the void ratio as the f_c increases. In this regime, the fines progressively disperse the coarse
145 particles, thereby causing an increase in the void ratio. These two regimes have been reported
146 in previous studies involving gap graded materials (Cubrinovski & Ishihara, 2002; Kuerbis,
147 1989; Lade & Yamamuro, 1997; W. Li et al., 2023; Y. Li et al., 2022; Minh et al., 2014; Sufian
148 et al., 2021; Vallejo, 2001; Zuo & Baudet, 2015). The two identified regimes are referred to as
149 the underfilled and the overfilled categories by dam engineers (ICOLD, 2013; Shire et al.,
150 2014), and are demarcated by the threshold fines content (i.e. the filled state).

151 One particular feature that is less frequently highlighted in the literature is the fact that the f_c^{th}
152 slightly depends on the relative density of the mixture. The f_c^{th} here was attained at $f_c = 0.30$
153 for the dense assemblies whereas $f_c^{th} = 0.35$ for the loose assemblies. Indeed, in looser
154 assemblies, the pores are larger and more fine grains are required to fill the voids before the
155 coarse grains are dispersed. This is in agreement with the 3D DEM study of binary mixtures
156 by Minh et al., (2014). In the literature, different limits within which the threshold fines content
157 is attainable have been reported. For example, Skempton & Brogan (1994) suggested that in
158 practice, f_c^{th} is unlikely to occur beyond 24% and 29% for dense and loose packings of sandy-
159 gravels, respectively. Lade & Yamamuro (1997) suggested a limit of 20%-30% fines content
160 for sand-silt mixtures of different gradations. Other studies show that the f_c^{th} can occur outside
161 Skempton and Brogan's and Lade & Yamamuro's limits, depending on the grain size
162 distribution and the particle shape considered (Evans & Zhou, 1995; Sarkar et al., 2020; Shire
163 et al., 2014; Sufian et al., 2021; Wang et al., 2022; Zuo & Baudet, 2015).

164 The conceptual distinction between underfilled and overfilled assemblies led Yin et al., (2014)
 165 to propose the following equation for determining the void ratio, e , for sand-silt mixtures at
 166 different fines content f_c :

$$167 \quad e = [e_{hc}(1 - f_c) + af_c] \frac{1 - \tanh[\xi(f_c - f_{th})]}{2} + e_{hf} \left(f_c + \frac{1 - f_c}{(R_d)^m} \right) \frac{1 + \tanh[\xi(f_c - f_{th})]}{2} \quad (1)$$

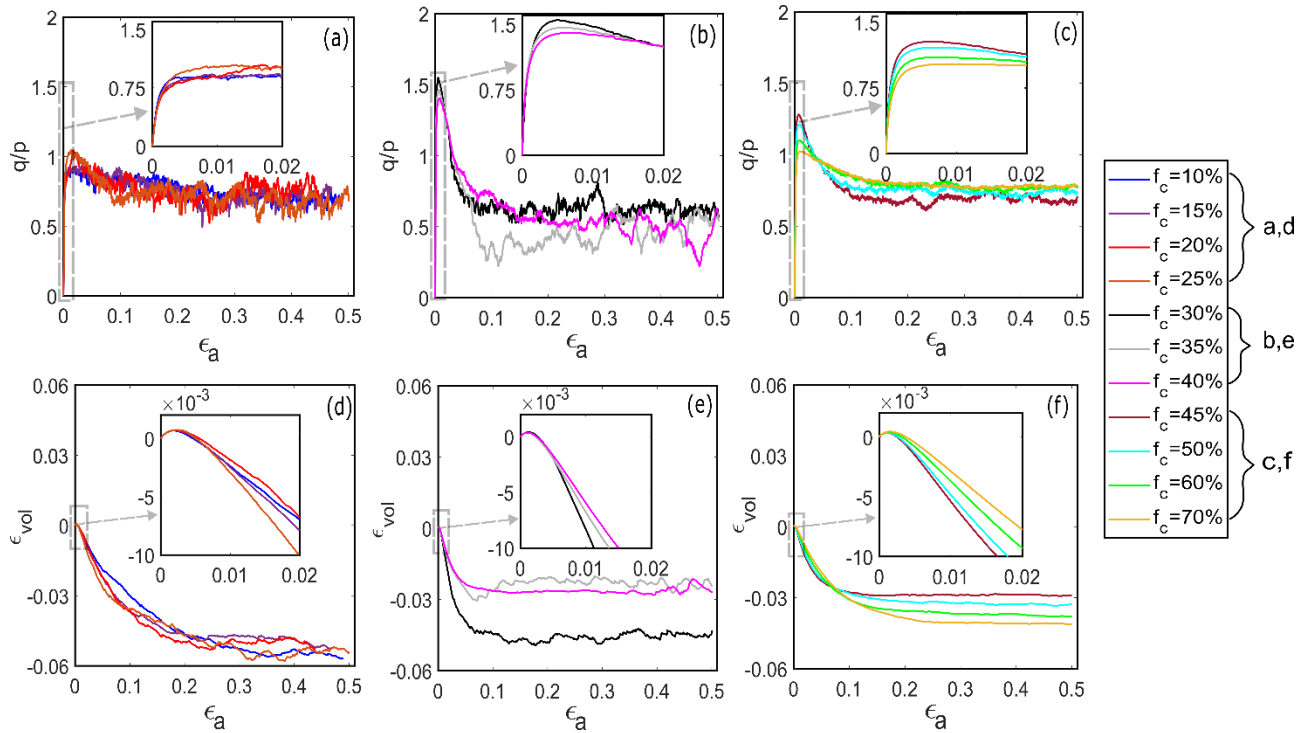
168 where e_{hc} is the void ratio of the pure sand, e_{hf} is the void ratio of the pure silt, a is a material
 169 constant depending on the fabric structure of the soil mixture, ξ is a material constant
 170 controlling the transition from a coarse grain matrix to a fine grain matrix, f_{th} is the threshold
 171 fines content at which the coarse and fine grains contribute equally to the global void ratio, R_d
 172 is the ratio of the mean size of the coarse grains, D_{50} , to the mean size of the fine grains d_{50}
 173 and m ($0 < m < 1$) is a coefficient that depends on grain characteristics and fine grain packing.
 174 The fitting parameters for the dense assemblies are $e_{hc} = 0.67; a = -0.64; \xi = 16.6; f_{th} = 0.28;$
 175 $e_{hf} = 0.62; m = 0.73$ while the parameters for the loose assemblies are $e_{hc} = 0.71; a = 0.03; \xi$
 176 $= 12.6; f_{th} = 0.26; e_{hf} = 0.76; m = 0.99$. It is clear, as shown in Fig. 2a, that this
 177 phenomenological equation fits our data.



178
 179 **Fig. 2.** Effect of fines content, f_c , on (a) the initial void ratio, e , (b) the range of attainable void
 180 ratios, $e_{max} - e_{min}$ for the assemblies of binary mixture studied
 181

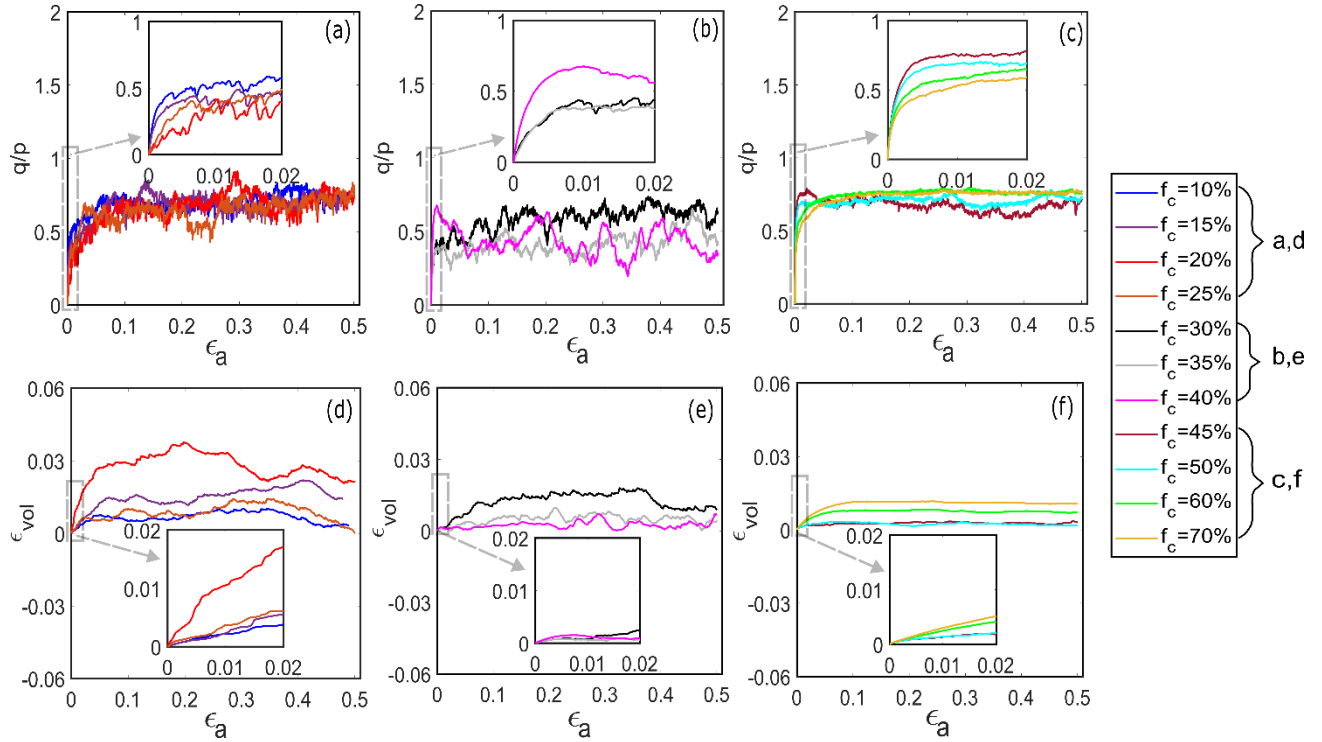
182 Fig. 2b shows the range of attainable void ratio, $e_{max} - e_{min}$, for each fines content. $e_{max} -$
 183 e_{min} for the underfilled assemblies (i.e. $f_c < f_c^{th} = 35\%$) is generally higher in comparison to
 184 the overfilled assemblies. In the underfilled assemblies, we observed an initial increase in
 185 $e_{max} - e_{min}$ with the fine content which indicates that the fines do not simply fill the voids in
 186 the loose case. Indeed, they enable the formation of larger pore structures.

187 Fig. 3 shows the evolution of the stress ratio, q/p , and the volumetric strain (ϵ_{vol}), against the
188 axial strain (ϵ_a), for the dense assemblies of binary mixtures with different fines content. The
189 corresponding data for the loose assemblies are presented in Fig. 4. The assemblies were
190 sheared until $\epsilon_a \approx 0.5$ in order to reach the critical state. Here, the deviatoric stress, $q = \sigma_{zz} -$
191 $(\sigma_{yy} + \sigma_{xx})/2$ and the mean stress, $p = (\sigma_{zz} + \sigma_{yy} + \sigma_{xx})/3$ (axisymmetric conditions). In a
192 typical fashion to sand behaviour, the q/p for the initially dense assemblies increased until
193 reaching a peak and thereafter softened to the critical state where the q/p fluctuates around a
194 mean value, with more pronounced fluctuations observed for $f_c < 45\%$ (Fig. 3a &b). The
195 stiffness of the packings as influenced by the fines content is shown in the inset of Fig. 3a-c.
196 These dense assemblies exhibited a dilative volumetric response ($\epsilon_{vol} < 0$) during shearing
197 (Fig. 3d-f). At large strains ($\epsilon_a > 35\%$), ϵ_{vol} tend to increase from $f_c = 10\%$ to $f_c = 35\%$
198 (indicating a less dilative behaviour), and then decreased with further increase in the f_c . In
199 contrast, at small strains ($\epsilon_a < 2\%$) (inset of Fig. 3d-f), a more dilative response was observed
200 from $f_c = 10\%$ to $f_c^{th}=30\%$ as ϵ_{vol} decreases. The stress ratio q/p for the initially loose
201 assemblies (Fig. 4a-c) increased monotonically from the beginning of shearing to the critical
202 state without significant softening observed, as expected. These loose assemblies exhibited a
203 contractive response ($\epsilon_{vol} > 0$) during shearing (Fig. 4d-f).



204

205 **Fig. 3.** Effect of fines content, f_c , on the stress-strain and the volumetric strain responses for
206 dense assemblies (a,d) $f_c = 10\%$ - 25% (b,e) $f_c = 30\%$ - 40% (c,f) $f_c = 45\%$ - 70% . Inset graphs
207 correspond to the start of the loading.

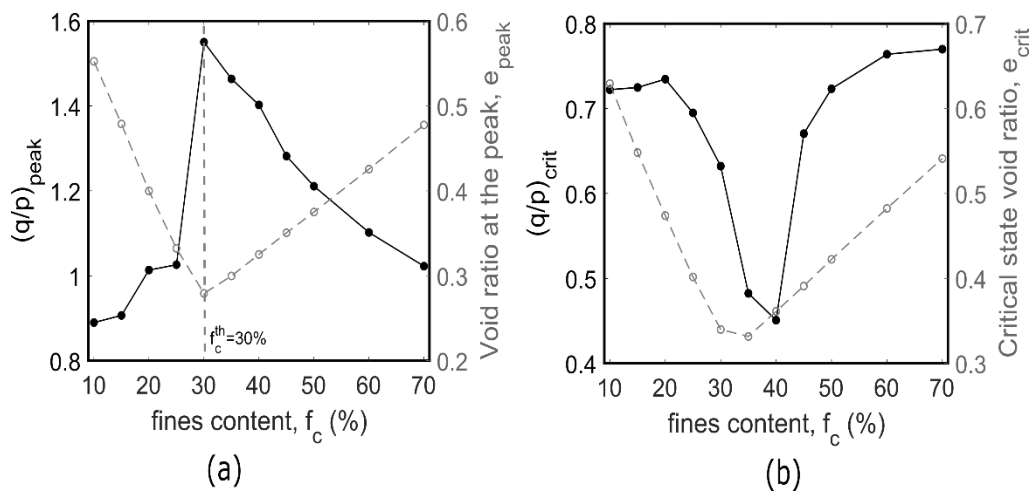


208
 209 **Fig. 4.** Effect of fines content, f_c , on the stress-strain and the volumetric strain responses for loose assemblies (a,d) $f_c = 10\%$ - 25% (b,e) $f_c = 30\%$ - 40% (c,f) $f_c = 45\%$ - 70% . Inset graphs
 210
 211 correspond to the start of the loading.
 212

213 In Fig. 5a, the stress ratio q/p at the peak, $(q/p)_{peak}$, is plotted against f_c alongside the void
 214 ratio at the peak, e_{peak} , for comparison. Similarly, Fig. 5b shows the plot of the critical state
 215 stress ratio, $(q/p)_{crit}$, against f_c alongside the critical state void ratio, e_{crit} . Here, the
 216 $(q/p)_{peak}$ is the maximum q/p attained between the start of shearing and the critical state;
 217 $(q/p)_{crit}$ and e_{crit} are mean values determined from the start of the critical state to the end of
 218 shearing. The critical state marks the state at which there is no noticeable change in the void
 219 ratio or the volume of a sample during shearing. This generally occurred at $\epsilon_a > 0.35$ for the
 220 studied assemblies. As the fines progressively fill the voids within the coarse particles in the
 221 underfilled regime where $f_c < f_c^{th}$, the assemblies become denser such that $(q/p)_{peak}$ increases
 222 with f_c until the threshold fines content where the highest $(q/p)_{peak}$ is attained (Fig. 5a). For
 223 $f_c > f_c^{th}$, the fines disperse the coarse particles leaving more voids within the assemblies thereby
 224 causing a monotonic decrease in $(q/p)_{peak}$ as f_c increased.

225 In agreement with earlier experimental studies on Ottawa sand and Carmague silty sand with
 226 $f_c \leq 20\%$ under drained shearing (Benahmed et al., 2015; Chang & Yin, 2011; Salgado et al.,
 227 2000), a marginal increase in $(q/p)_{crit}$ was observed from $f_c = 10\%$ to $f_c = 20\%$. This is
 228 followed by a significant decrease in $(q/p)_{crit}$ until $f_c = 40\%$, and finally a monotonic increase

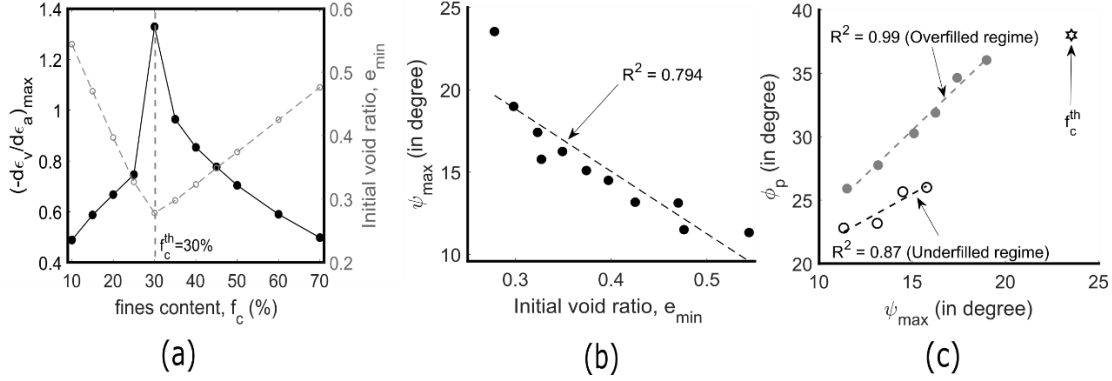
229 until $f_c = 70\%$ (Fig. 5b). The e_{crit} follows a similar trend as the e_{peak} , although the threshold
 230 fines content shifted from $f_c^{th}=30\%$ at the initial state (Fig. 5a) to $f_c^{th}=35\%$ at the critical state
 231 (Fig. 5b). While e_{peak} could be used to explain the trend observed for $(q/p)_{peak}$, $(q/p)_{crit}$
 232 does not correlate with e_{crit} . In Section 6, we provide a discussion on the use of an alternative
 233 void index, the stress-based skeleton void ratio, to explain the trend observed at the critical
 234 state. It is worthy of note that having a lot of fine grains filling the void space increases the
 235 peak strength but decreases the critical state strength. This might be interpreted in the capacity
 236 of fine grains to i) provide lateral support to force chains if the initial state is dense, but at the
 237 same time ii) act as ball bearings at critical state and ease shearing with limited deviatoric
 238 stress.



239 **Fig. 5** Effect of fines content on (a) stress ratio at peak, $(q/p)_{peak}$, for the dense assemblies,
 240 and peak void ratio, e_{peak} (b) critical state stress ratio, $(q/p)_{crit}$, (unique value for dense and
 241 loose assemblies), and critical state void ratio, e_{crit} .
 242
 243

244 Fig. 6a shows the maximum dilatancy rate, $(-d\varepsilon_v/d\varepsilon_a)_{max}$ against f_c . In the underfilled
 245 regime, $(-d\varepsilon_v/d\varepsilon_a)_{max}$ for the dense assemblies increased from $f_c = 10\%$ until the threshold
 246 fines content $f_c^{th}=30\%$, as the fines progressively fill the void space (Fig. 6a). For $f_c > f_c^{th}$,
 247 $(-d\varepsilon_v/d\varepsilon_a)_{max}$ decreased monotonically with an increase in f_c . The increase in dilatancy
 248 observed within the underfilled regime was also reported for Ottawa sand having $f_c \leq 20\%$,
 249 under drained triaxial shearing (Chang & Yin, 2011; Salgado et al., 2000); and was attributed
 250 to increased particle interlock as the fines occupy the voids within the coarse particles (Kuerbis,
 251 1989; Salgado et al., 2000). Indeed, for the assemblies of binary mixture studied here, there is
 252 a correlation between the maximum dilatancy angle, ψ_{max} and the initial void ratio, e_{min} , (Fig.
 253 6b), where $\psi_{max} = \sin^{-1} [(-d\varepsilon_v/d\varepsilon_a)_{max} / (2 + (-d\varepsilon_v/d\varepsilon_a)_{max})]$ following (Xiao et al.,
 254 2017). A linear relationship was also established between the peak friction angle, ϕ_p and the

255 ψ_{max} (Fig. 6c), where the friction angle, $\phi = \sin^{-1}[(\sigma_{zz} - \sigma_{yy})/(\sigma_{zz} + \sigma_{yy})]$. This
 256 relationship has been found in earlier studies for clean sands (Adesina et al., 2024; Bolton,
 257 1986; Vaid & Sasitharan, 1992), and was also reported for sand-silt mixtures having $f_c \leq 20\%$
 258 in the experimental study on sand with non-plastic fines (Xiao et al., 2017).



259 (a) Effect of fines content, f_c , on the maximum dilatancy rate, $(-d\varepsilon_v/d\varepsilon_a)_{max}$.
 260 Relationship between (b) maximum dilatancy angle, ψ_{max} and initial void ratio, e_{min} (c) peak
 261 friction angle, ϕ_p , and maximum dilatancy angle, ψ_{max} for dense assemblies of binary mixture.
 262
 263

264 The coordination number, i.e. the average number of contacts per particle in a granular system
 265 is the simplest measure of the connectivity of the contact network which is related to the
 266 structural stability of the system (Thornton, 2015). Here, we employ the mechanical
 267 coordination number as a micromechanical parameter to identify and characterise the regimes
 268 delineating the behaviour of gap-graded materials. The mechanical coordination number, Z_m ,
 269 is defined as the average number of contacts per particle when the particles which do not
 270 contribute to force transmission (i.e., particles with less than two contacts which are referred
 271 to as rattlers) are excluded⁷. Thornton (2000) defined the Z_m as:

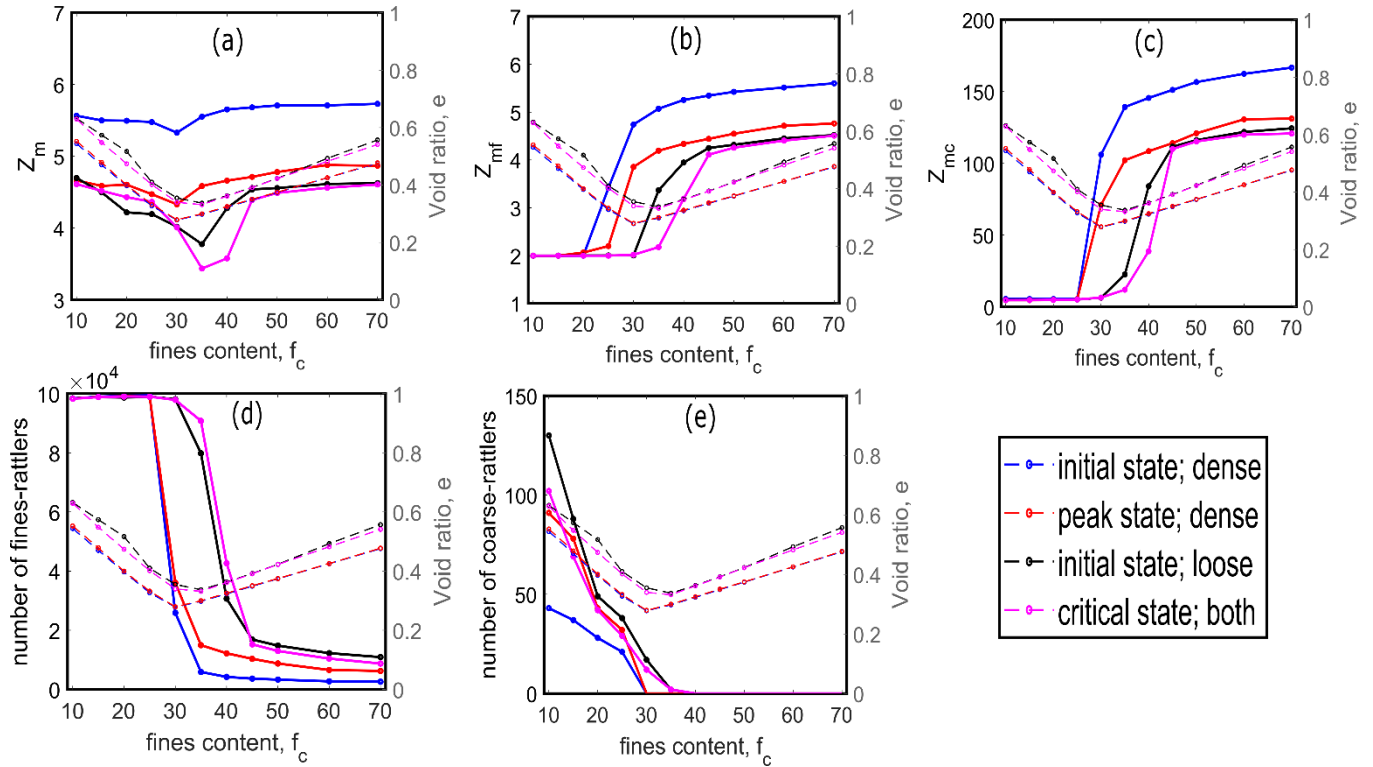
$$272 \quad Z_m = \frac{(2N_c - N_1)}{N_p - N_1 - N_0} \quad (2)$$

273 where N_c is the total number of contacts, N_p is total number of particles and N_0 and N_1 are the
 274 number of particles with zero and one contact in the granular system, respectively. Figs. 7a-c
 275 show Z_m for all particles, Z_{mc} for the coarse particles only, and Z_{mf} for the fine particles only,
 276 respectively, alongside the void ratio, e , at the initial, the peak and the critical states. While Z_m
 277 considers all particles, Z_{mc} and Z_{mf} considers only the contacts made by the coarse particles
 278 and the fine particles, respectively⁸. Figs. 7d-e show the number of fines and coarse particles

⁷ Note that the coordination number of particles with more than two contacts accounts for the contacts from particles with only one contact in the standard definition of Z_m .

⁸ The contacts made by the coarse particles include both the coarse-coarse and the coarse-fine contacts while the contacts made by the fine particles include both the fine-fine and the coarse-fine contacts.

279 that do not contribute to force transmission (i.e. the fines-rattlers and coarse-rattlers) at the
 280 initial, the peak and the critical states. Generally, two trends demarcated by the f_c^{th} can be
 281 observed in Fig. 7a; a decrease in the Z_m for $f_c < f_c^{th}$ (although the decrease is less significant
 282 for the dense assemblies at the initial state); and a monotonic increase for $f_c > f_c^{th}$. The trends
 283 observed here are similar to the data shown in the DEM study by Liu et al., (2022) for the Z_m
 284 of sand-silt mixtures having particle size ratio, $\lambda = 8.4$ and 18.1, and at the initial states.
 285 Generally, an initial increase in the f_c resulted in no change in the Z_{mc} and the Z_{mf} until f_c^{th} ,
 286 after which a monotonic increase followed (Figs. 7b & c). The monotonic decrease in the
 287 number of fines-rattlers from f_c^{th} (Fig. 7d) indicates an increase in the number of fines
 288 mobilised in force transmission as f_c increases. As expected, the number of coarse-rattlers
 289 decreased with an increase in f_c until f_c^{th} , beyond which no rattler exists among the coarse
 290 particles (Fig. 7e).

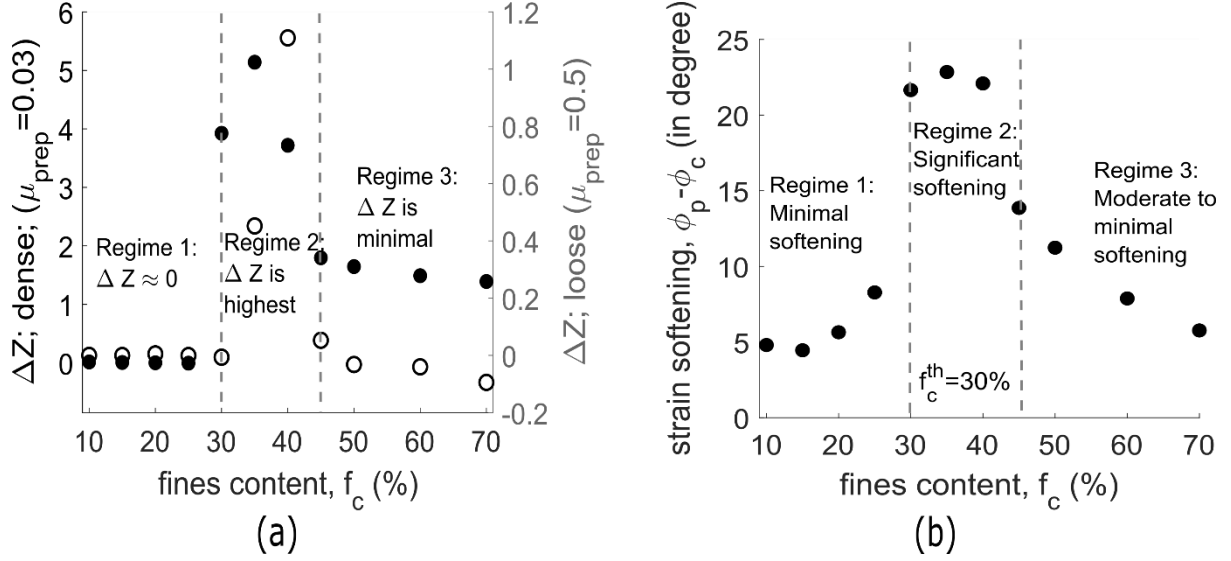


291
 292 **Fig. 7** Effect of fines content on the (a) mechanical coordination number, Z_m , for all particles
 293 (b) Z_{mc} for coarse particles (c) Z_{mf} for fine particles (d) number of fines-rattlers (e) number of
 294 coarse-rattlers within assemblies of binary mixture.

295
 296 Fig. 8a shows the contact lost or gained during shearing, ΔZ , determined here as $Z_{ini} - Z_{crit}$,
 297 where Z_{ini} and Z_{crit} are the coordination number at the initial states and at the critical state,
 298 respectively. Fig. 8b shows the excess friction angle, which indicates the strain softening
 299 exhibited by the assemblies. From these figures, we observe the emergence of three groups of

300 f_c values with similar ΔZ and $\phi_p - \phi_c$ values. This suggests the existence of three regimes, the
301 first being $f_c < f_c^{th}$ where $\Delta Z \approx 0$ and strain softening is relatively minimal. In the second
302 regime delineated by $f_c^{th} \leq f_c < 45\%$, ΔZ is highest, suggesting that the highest amount of
303 contacts were lost within this regime during shearing. This is accompanied by significant
304 softening occurring within the regime, in agreement with the DEM study by Adesina et al.,
305 (2024), where a linear relationship is established between the degree of softening and the
306 contact loss during shearing by linearly-graded granular assemblies. The significant loss of
307 contacts exhibited by the assemblies in this regime can be linked to the large fluctuations in
308 their shearing responses at the critical state (see Figs. 3 & 4). It has been shown in the DEM
309 study by Adesina et al., (2022) that the magnitude of fluctuations in the shearing responses of
310 granular assemblies at the critical state increases with a decrease in the total number of contacts
311 in the assemblies. This observation can also be related to the size of the REV, which depends
312 on the fine contents. While the condition is largely met for small and large fine contents with
313 100,000 grains, this is less the case for intermediate fine contents in which local microstructure
314 rearrangements reflect more in the macroscopic response. This is observed in Fig. 16 through
315 the evolution of the boundary term in the stress decomposition. In Appendix A, we showed that
316 our sample size of 100,000 particles can be considered as a REV.

317 In the third regime (i.e. $f_c \geq 45\%$), relatively minimal ΔZ is observed; the strain softening
318 within this regime transitions from moderate to minimal. ΔZ values in the last two regimes are
319 higher for dense assemblies in comparison to the loose assemblies, for the same f_c value; $\Delta Z < 0$
320 for the loose assemblies in regime 3 indicating an ultimate contact gain. While Skempton &
321 Brogan (1994) and Thevanayagam et al., (2002) provided a conceptual delineation of the
322 regimes based on void ratio, here, we provide a mechanistic delineation of the regimes with
323 our analysis of contact evolution and strain softening. In Table 3, we present a summary of the
324 unique trends observed for each of the three regimes identified based on our analysis of the
325 macromechanical and the micromechanical characteristics of the studied gap-graded
326 assemblies.



327 **Fig. 8** (a) Change in coordination number during shearing, ΔZ (filled circle for dense
 328 assemblies and open circles for loose assemblies). $\Delta Z > 0$ means contact lost and $\Delta Z < 0$ means
 329 contact gained during shearing. (b) excess friction angle (strain softening), $\phi_p - \phi_c$ for dense
 330 assemblies of binary mixture.
 331
 332

333 **Table 3:** Summary of regime based on macromechanical and micromechanical characteristics

Δ in parameters as the $f_c \uparrow$	Regime 1 ($f_c < f_c^{\text{th}}$)	Regime 2 ($f_c^{\text{th}} < f_c < 45\%$)	Regime 3 ($f_c > 45\%$)
$e_{\text{ini}}; e_{\text{crit}}$	Decreases		Increases
$(q/p)_{\text{max}}$	Increases		Decreases
$(-d\varepsilon_v/d\varepsilon_a)_{\text{max}}$	Increases		Decreases
Z_m	Decreases	Increases	Increases marginally to a plateau
$Z_{mc}; Z_{mf}$	No change	Increases	Increases marginally to a plateau
ΔZ	No change	Increases	Decreases marginally to a plateau
$\phi_p - \phi_c$	Increases	Plateau	Decreases

334 Note: When the data in Fig. 8 are considered, the boundary between Regime 2 and Regime 3 range between $f_c \in$
 335 $[35\% ; 45\%]$ depending on density. This range will also depend on the particle size distribution considered.
 336

337 4. Particle based stress-transmission

338
 339 Using the Love-Weber particle stress tensor as described in Nicot et al., (2013), the mean stress
 340 per particle, σ_{ij}^p , is calculated as:

$$341 \quad \sigma_{ij}^p = \frac{1}{V_p} R_p \sum_{c=1}^{N_c^p} f_j^c \mathbf{n}_i \quad (3)$$

342 where the summation runs over all contacts c made by the particle p . V^p is the particle volume,
 343 R_p is the radius of the particle, N_c^p is the number of contacts involving the particle, f_j^c is the
 344 contact force vector and \mathbf{n}_i is the unit branch vector between two particles in contact. The stress
 345 tensor at the material point scale (i.e. for a large number of particles), σ_{ij} , is given as a weighted
 346 average of the particle stresses (by particle volume):

$$347 \quad \sigma_{ij} = \frac{1}{V} \sum_{p=1}^{N_p} V^p \sigma_{ij}^p \quad (4)$$

348 where V is the volume of the entire system and N_p is the number of particles in the system.
 349 σ_{ij} can be decomposed to the contribution of each particle category, i.e. fine and coarse, as:

$$350 \quad \sigma_{ij} = \underbrace{\frac{1}{V} \sum_{p=1}^{N_p^c} V^p \sigma_{ij}^p}_{\sigma_{ij}^c} + \underbrace{\frac{1}{V} \sum_{p=1}^{N_p^f} V^p \sigma_{ij}^p}_{\sigma_{ij}^f} \quad (5)$$

351 where N_p^c and N_p^f are the number of coarse and fine particles in the system, respectively⁹. The
 352 mean effective stress, p , for the entire system is calculated as:

$$353 \quad p = \frac{\sigma_{xx} + \sigma_{yy} + \sigma_{zz}}{3} \quad (6)$$

354 The proportion of the total mean stress transmitted by the finer fraction, α_f , is calculated as
 355 p^f/p , and similarly, the proportion of the total mean stress transmitted by the coarser fraction,
 356 $\alpha_c = 1 - \alpha_f$, is calculated as p^c/p , where p^f and p^c are the mean stress transmitted by the
 357 finer and the coarser populations, respectively.

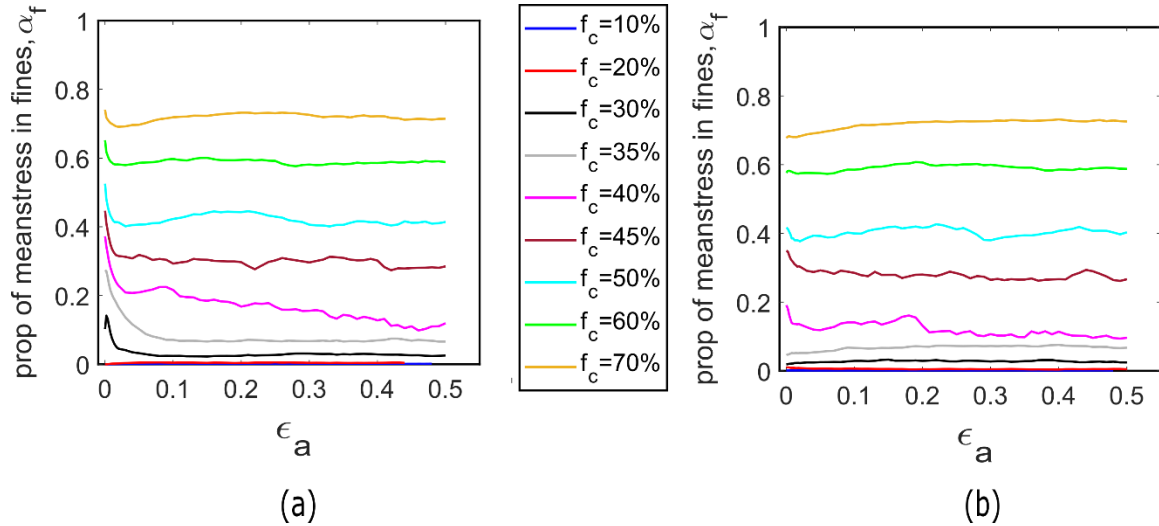
358 Fig. 9 shows the evolution of the α_f during shearing for the dense and loose assemblies of
 359 binary mixtures¹⁰. The α_f for the dense assemblies having $f_c \geq 30\%$ decreased significantly
 360 (with more pronounced decrease observed for $35\% \leq f_c \leq 50\%$ which corresponds with regime
 361 2 in Table 3) from the start of shearing until $\epsilon_a \approx 0.08$ beyond which the change in the α_f
 362 became minimal (Fig. 9a). α_f for the loose assemblies generally exhibited minimal changes
 363 from the start to the end of shearing (Fig. 9b). In agreement with the data presented by Sufian
 364 et al., (2021) for sand-silt mixtures subjected to constant mean stress triaxial compression, the

⁹ Note that σ_{ij}^c and σ_{ij}^f correspond to the contribution of coarse and fine particles to the total stress and not to the mean stress in coarse and fine particles. To compute the stress in the coarse particles, we consider both the coarse-coarse and the coarse-fine contacts. Similarly, to compute the stress in the fine particles, we consider both the fine-fine and the coarse-fine contacts.

¹⁰ In Appendix B and Fig. A2, we show that the evolution of the deviatoric stress transmitted by the fines is generally similar to the evolution of the mean stress presented in Fig. 8.

365 observation made here indicates the transmission of stresses from the fine particles to the coarse
 366 particles or a concentration of stress on the coarse particles, in the dense assemblies, at the early
 367 stage of shearing. This phenomenon occurred such that for each f_c , a unique α_f exists for both
 368 the initially dense and loose assemblies at large strains (i.e. at the critical state).

369



370

371

Fig. 9 Evolution of the proportion of mean stress transmitted by the fines during shearing for (a) dense assemblies (b) loose assemblies¹¹

372

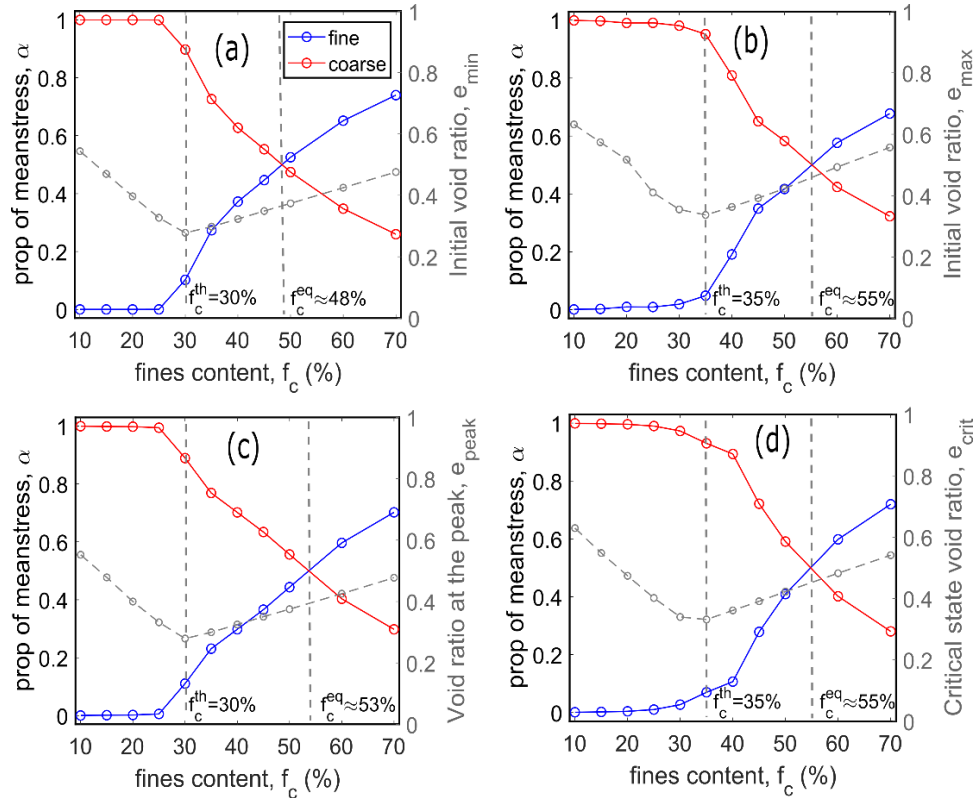
373

374 Fig. 10 shows the contribution of the finer fraction, α_f , and the coarser fraction, α_c , to the total
 375 mean stress for the studied assemblies. At all stages of shearing considered (Fig. 10a-d), the
 376 fine particles did not contribute to stress transmission (i.e. $\alpha_f \approx 0$) until the f_c^{th} beyond which
 377 there was a progressive increase in the α_f and a consequential reduction in α_c . The primary
 378 stress-transmitting skeleton at $f_c < f_c^{th}$ is therefore the coarser fraction. Based on a conceptual
 379 analysis proposed in the experimental studies on granular mixtures (Thevanayagam et al.,
 380 2002; Thevanayagam & Mohan, 2000), the mechanical behaviour of the mixtures should be
 381 primarily controlled by the fines at $f_c \geq f_c^{th}$. Vallejo (2001) in his experimental study on binary
 382 granular mixtures suggests that at $f_c > 60\%$, the fines generally become the primary stress-
 383 transmitting matrix while the coarser fraction plays basically no role in stress transmission. The
 384 evidence from our micromechanical analysis shows that while the fines began to transmit stress
 385 at the f_c^{th} , they did not become the primary stress-transmitting fabric until f_c becomes higher
 386 than an equivalent fines content f_c^{eq} . Here, f_c^{eq} is the estimated f_c at which the total mean

¹¹ By comparing the q/p data (Figs. 3 & 4) with the α_f data (Fig. 9), it is observed that the fluctuation in the q/p data for the assemblies having $f_c \in [30\% ; 40\%]$ is not reflected in the relatively smooth α_f data. This is because the fluctuations evident in the q/p data is masked behind the apparently smooth α_f data as a result of the normalisation of the stress transmitted by the fines with the total mean stress (p^f/p).

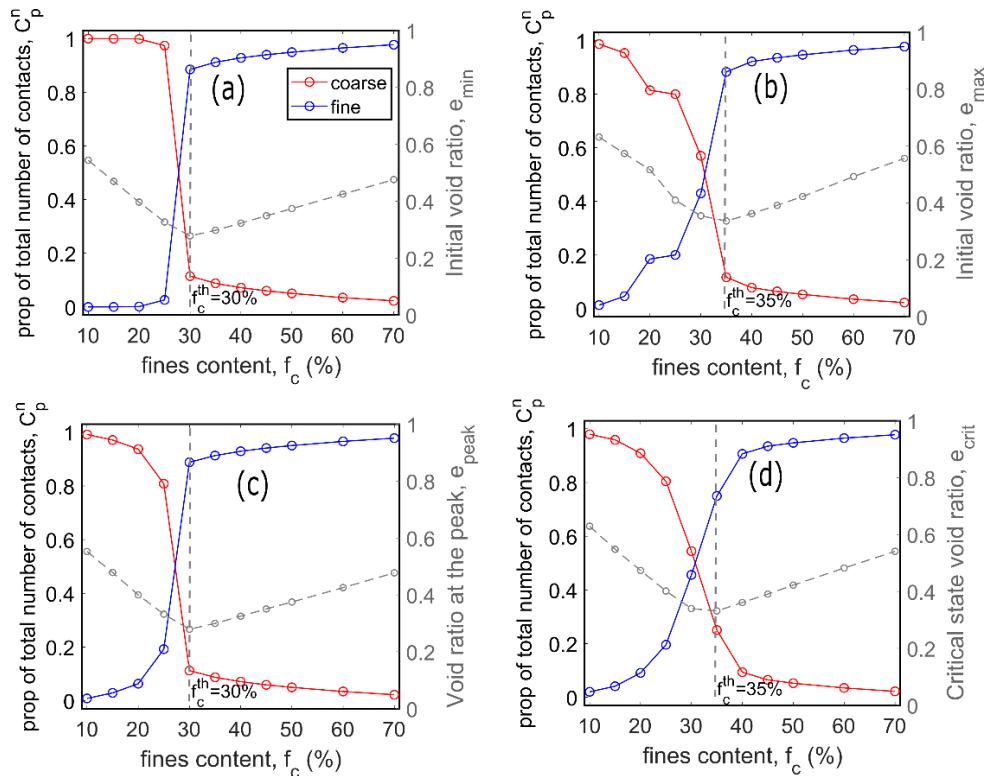
387 pressure is equally shared between the finer and the coarser fraction. For the studied binary
 388 mixtures, f_c^{eq} is estimated to range from 48% to 53% for the dense assemblies at the initial
 389 state and the peak; and reaches 55% for the loose assemblies at the initial state and for all
 390 assemblies at the critical state. Contrary to Vallejo (2001), while the fines transmit the largest
 391 fraction of the total mean stress for $f_c > f_c^{eq}$, the coarse particles continue to make a secondary
 392 and yet significant contribution to the total mean stress for much larger fine contents (at least
 393 up to $f_c=70\%$ studied here).
 394 Since particles stresses result from contact forces, we estimate in Fig. 11, the proportion of the
 395 total number contacts shared by the fines¹², C_n^f , and the coarse particles, C_n^c . Comparing these
 396 geometric statistics to the stress contributions enables a better understanding of the trends
 397 observed in Fig. 10. Again, the trends in Fig. 11 can be classified into two regimes delineated
 398 by the threshold fines content, f_c^{th} . For $f_c < f_c^{th}$, C_n^f generally increased with f_c but remained
 399 lower than C_n^c , indicating that in this regime, the coarse particles are involved in a larger
 400 proportion of the total number of contacts than the fines. For $f_c \geq f_c^{th}$, C_n^f increased
 401 monotonically with f_c and was higher than C_n^c ; in this case, the fines became dominant in terms
 402 of their proportion of the total number of contacts. By comparing Fig. 10 and 11, we observe
 403 that although the fines became dominant in terms of their proportion of the total number of
 404 contacts from $f_c = f_c^{th}$, they did not primarily contribute to the total mean stress until $f_c > f_c^{eq}$.
 405 This indicates that most of the contacts involving fine grains do not carry large forces for
 406 $f_c^{th} < f_c < f_c^{eq}$.

¹² The contacts made by the coarse particles include both the coarse-coarse and the coarse-fine contacts while the contacts made by the fine particles include both the fine-fine and the coarse-fine contacts. The proportion of the total number of contacts shared by the fines, C_n^f , is calculated as: $C_n^f = \frac{2N_{f-f} + N_{c-f}}{2N_{f-f} + 2N_{c-f} + 2N_{c-c}}$.



407
408
409
410
411

Fig. 10 Proportion of mean stress transmitted by the fines and coarse particles at (a) the initial state for dense assemblies (b) the initial state for the loose assemblies (c) the peak (d) the critical state (unique trends for both dense and loose assemblies)



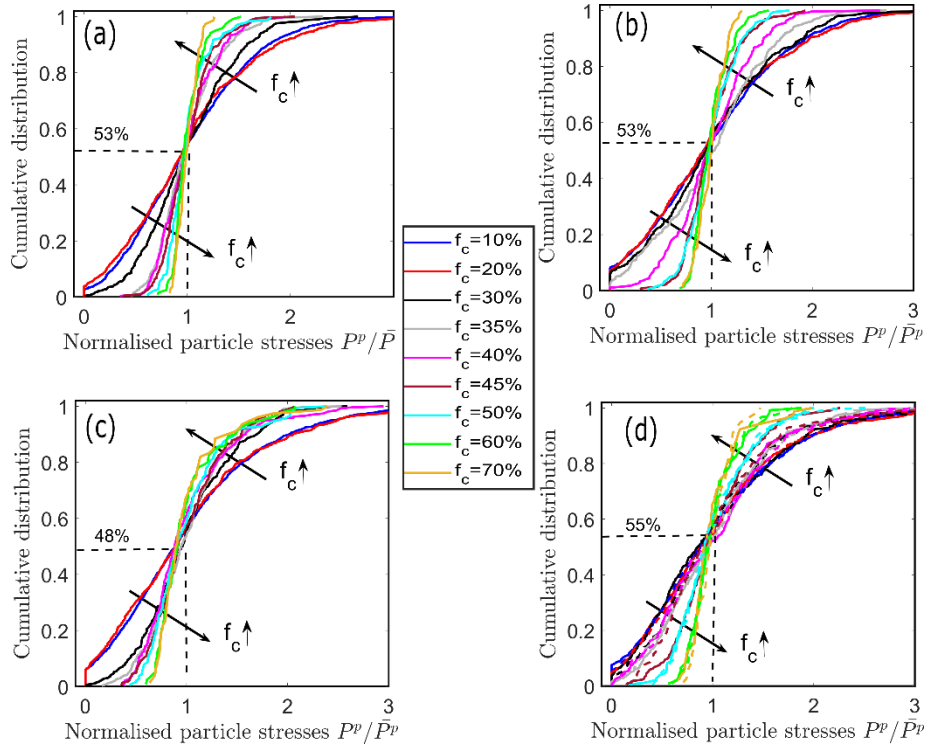
412
413
414
415
416

Fig. 11 Proportion of the total contacts belonging to the finer and coarser fraction at (a) the initial state for dense assemblies (b) the initial state for the loose assemblies (c) the peak (d) the critical state (unique trends for both dense and loose assemblies)

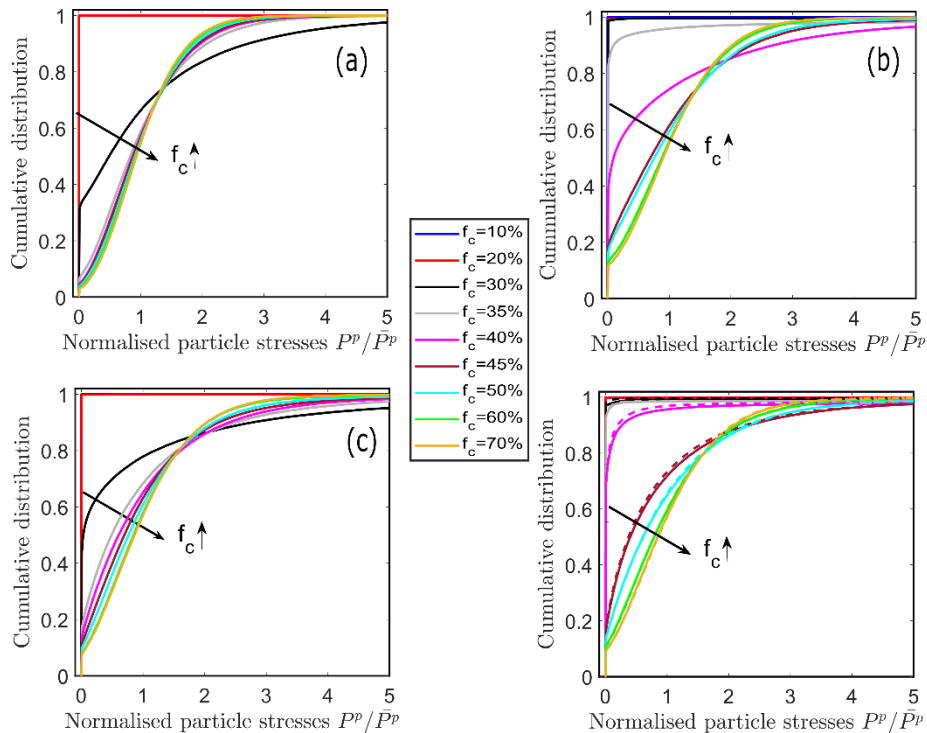
417 Figs. 12 and 13 show the cumulative distributions of the individual stresses sustained by the
 418 particles normalised by the average particle stresses in the whole assembly ($P^p/\overline{P^p}$), for the
 419 coarser and finer fraction respectively, at the initial states, the peak and the critical state. This
 420 is aimed at understanding the range and state of particle stresses existing within the particle
 421 size fractions in each assembly at different shearing stages. A wider range of stresses exist
 422 within the finer fraction (Fig. 13) than the coarser fraction (Fig. 12). For the coarser fraction,
 423 the proportion of the particles with stress values below the average stress (i.e. $P^p/\overline{P^p} \leq 1$) was
 424 similar for all f_c values considered. Below the average stress, the cumulative distribution shifts
 425 to the right as f_c increased; the reverse was observed above the average stress. The width of
 426 the distributions for the coarser fraction tend to become smaller as f_c increased (Fig. 12a-d).
 427 This indicates a more even stress distribution within the coarser particles as f_c increased. The
 428 proportion of the fines with stress values below the average (i.e. $P^p/\overline{P^p} \leq 1$) decreased as f_c
 429 increased (Fig. 13).

430 The proportion of the fines bearing no stress (i.e. $P^p/\overline{P^p} = 0$), referred to as the non-active
 431 fines, R_f , are illustrated by the vertical line at $P^p/\overline{P^p} = 0$ in Fig. 13 and are plotted in Fig. 14a.
 432 Fig. 14b shows the change in the percentage of the non-active fines present within the
 433 assemblies during shearing, ΔR_f (i.e. the difference in the R_f at the initial states and the critical
 434 state). Within the assemblies having $f_c < f_c^{th}$, virtually all the fines (98.3% to 99.9%) are non-
 435 active. This confirms that at $f_c < f_c^{th}$, the finer fraction does not contribute to stress transfer. For
 436 $f_c^{th} < f_c < 45\%$, R_f decreases more significantly than for $f_c > 45\%$ (Fig. 14a). The drop in the
 437 proportion of non-active fine (within $f_c^{th} < f_c < 45\%$) depends significantly on the relative
 438 density of the assemblies (dense or loose) and the stage of shearing (initial, peak or critical
 439 state). Three regimes are identified following the analysis here. For $f_c < f_c^{th}$, the fines are largely
 440 dormant whatever the sample state¹³. Also, $\Delta R_f \approx 0$ (Fig. 14b), indicating shearing had no effect
 441 on the activity of the fines. For $f_c^{th} \leq f_c < 45\%$, the proportion of active fines is very sensitive
 442 to the packing density and the stage of shearing (Fig. 14a). Also, ΔR_f is highest (Fig. 14b),
 443 suggesting that more of the active fines initially present within the assemblies became non-
 444 active by the end of shearing (38%-85% and 11-12% for dense and loose assemblies,
 445 respectively). For $f_c \geq 45\%$, the proportion of non-active fines is rather low and exhibit a
 446 limited sensitivity to the packing density and the stage of shearing.

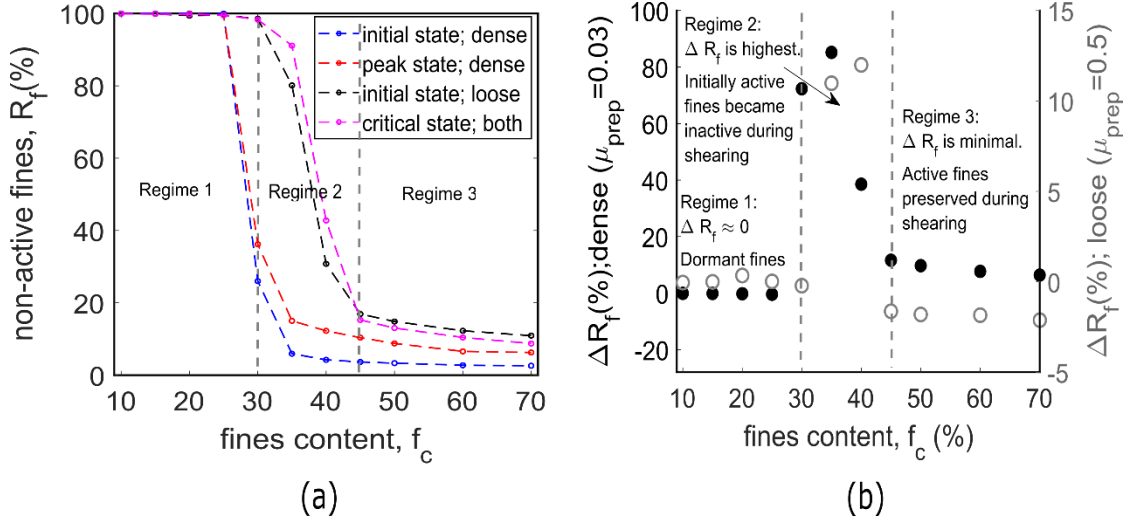
¹³ Note that, depending on the sample preparation procedure, we could imagine having fewer non-active fines at initial state. This is for instance the case when samples are prepared in the lab using the moist tamping method that gather fines around contacts between coarse grains because of capillary effects.



447
 448 **Fig. 12** Cumulative distribution of normalised particle mean stress for coarser fraction (a)
 449 dense; initial state (b) loose; initial state (c) dense; peak state (d) critical state for both dense
 450 (solid line) and loose (dashed line) assemblies
 451



452
 453 **Fig. 13** Cumulative distribution of normalised particle mean stress for finer fraction (a) dense;
 454 initial state (b) loose; initial state (c) dense; peak state (d) critical state for both dense (solid
 455 line) and loose (dashed line) assemblies
 456



457

458 **Fig. 14** (a) Percentage of non-active fines, R_f , at different f_c (b) Change in the percentage of
 459 non-active fines during shearing (filled circle for dense assemblies and open circles for loose
 460 assemblies). $\Delta R_f > 0$ and $\Delta R_f < 0$ mean higher and lower percentages of inactive fines at the end
 461 of shearing in comparison to the initial state, respectively.

462

463

464

465 5. Contact based stress-transmission

466

467 Using the Love-Weber contact based stress tensor including Bagi boundary term (Bagi, 1999),
 468 the contributions of all contact types to the total mean stress transmitted by an entire granular
 469 system is given as:

$$470 \quad \sigma_{ij}^c = \frac{1}{V} \sum_{c=1}^{N_c} f_j^c l_i \quad (11)$$

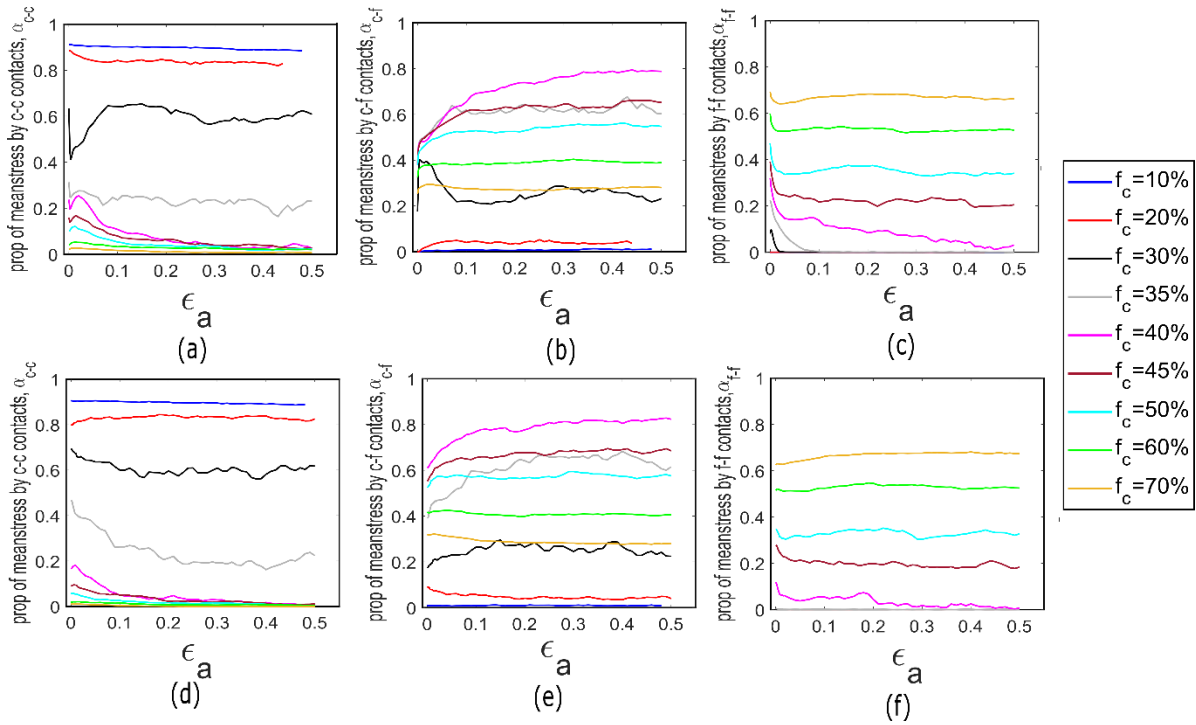
471 where N_c is the total number of contacts in the granular system, V is the volume of the system,
 472 \mathbf{l} is the branch vector ($\|\mathbf{l}\| = R_1 + R_2$ for a sphere 1 to sphere 2 contact; $\|\mathbf{l}\| = R_p$ for a sphere
 473 p to wall contact), and \mathbf{f}^c is the contact force vector. This stress tensor can be decomposed
 474 based on the contact type as:

$$475 \quad \sigma_{ij}^k = \frac{1}{V} \sum_{c=1}^{N_c^k} f_j^c l_i \quad (12)$$

476 where $k \in \{c-c, c-f, f-f, s-w\}$. c-c, c-f, f-f, and s-wl denote coarse to coarse, coarse to fine, fine
 477 to fine and sphere to wall contacts, respectively. The proportion of the total mean stress from
 478 each contact type is given by $\alpha_k = p^k / p$. Note that the boundary term is expected to vanish as
 479 soon as the sample domain is sufficiently large (which should be the case when the REV
 480 condition is met).

481 Fig. 15 shows the evolution of the proportion of the stress transmitted by each contact type
482 during shearing, for the dense and loose assemblies. At large strains (i.e., $\epsilon_a > 0.3$), the
483 contribution of the coarse to coarse contacts to the total mean stress, α_{c-c} , decreases with f_c
484 such that $\alpha_{c-c} \approx 0$ for $f_c > 40\%$ (Fig. 15a&d). The contribution of the fine-fine contacts to the
485 total mean stress, α_{f-f} , increases with f_c for $f_c > f_c^{th}$ while $\alpha_{f-f} \approx 0$ for $f_c < f_c^{th}$ (Fig. 15c&f).
486 The contribution of the coarse to fine contacts, α_{c-f} , initially increases with f_c until $f_c = 40\%$
487 and thereafter decreases with further increase in f_c (Fig. 15b&e). During the early stage of
488 shearing (i.e., $\epsilon_a < 0.1$), we observed a decrease in α_{c-c} and α_{f-f} which is accompanied by a
489 commensurate increase in the α_{c-f} . This indicates a redistribution of stress from the c-c and
490 f-f contacts to the c-f contacts. Although the coarse particles lost stress as indicated in the
491 decrease in α_{c-c} , they are also gained stress from the fines as indicated in both the increase in
492 α_{c-f} and the decrease in α_{f-f} . Ultimately, there was a redistribution of stress from the fines to
493 the coarse particles as indicated in Fig. 9a.

494



495

496 **Fig. 15** Evolution of the proportion of mean stress transmitted by contact types during shearing
497 for (a) c-c contacts; dense (b) c-f contacts; dense (c) f-f contacts; dense (d) c-c contacts; loose
498 (b) c-f contacts; loose (c) f-f contacts; loose

499

500 Fig. 16 shows the proportion of the mean stress transmitted by each contact types at the initial
 501 states, the peak and the critical state. The trends observed between the contact types¹⁴ can be
 502 classified into four regimes based on the f_c . In the first regime ($f_c < f_c^{th}$), the contribution of the
 503 fine to fine contacts to the total mean stress, $\alpha_{f-f} \approx 0$, indicating that the f-f contacts do not
 504 contribute to mean stress below the f_c^{th} . In this regime, the condition $\alpha_{c-c} > \alpha_{c-f} > \alpha_{f-f}$
 505 generally holds, hence, the regime is referred to as coarse-dominated, following Vallejo (2001)
 506 and Sufian et al. (2021). Within the second regime referred to as transitional coarse-dominated
 507 ($f_c^{th} < f_c < f_c^{tr}$, where f_c^{tr} is referred here as transitional fines content where $\alpha_{c-c} = \alpha_{f-f}$), the
 508 condition $\alpha_{c-f} > \alpha_{c-c} > \alpha_{f-f}$ generally holds. In the third regime where $f_c^{tr} < f_c < f_c^{eq}$ (f_c^{eq}
 509 was defined in Section 4 as the f_c at which the total mean stress is equally shared between the
 510 coarser and the finer fractions) and referred to as transitional fines-dominated, the condition
 511 $\alpha_{c-f} > \alpha_{f-f} > \alpha_{c-c}$ holds. The transitional fines content, f_c^{tr} , delineating the transitional
 512 regimes (i.e. the transitional-coarse dominated and the transitional-fines dominated regimes)
 513 was found around $f_c = 40\%$ for the assemblies and the shearing stages considered here (Fig.
 514 16a-d). The transitional regime based on the micromechanical analysis ranged from f_c^{th} to f_c^{eq}
 515 and is therefore within $f_c = 30\% - 48\%$ and $f_c = 35\% - 55\%$ for the dense and loose assemblies,
 516 respectively. For $f_c > f_c^{eq}$ (i.e., in the fourth regime), the condition $\alpha_{f-f} > \alpha_{c-f} > \alpha_{c-c}$ holds,
 517 hence, the regime is fines-dominated. While the classification in the experimental study by
 518 Vallejo (2001) was based on void ratio, we present here a similar classification based on the
 519 micromechanical analysis conducted, with distinct delineations in agreement with the 3-D
 520 DEM study on binary mixtures having size ratio, $\lambda = 4$, reported by Minh et al., (2014).

¹⁴ Excluding the contributions to the mean stress from the contacts between the spherical particles and the walls, α_{s-wl} , which were generally less than 0.15. We observed that α_{s-wl} values for the underfilled assemblies ($f_c < f_c^{th}$) were generally higher than the overfilled assemblies. This suggests that a greater number of particles is required to ensure a representative element volume (REV) in underfilled assemblies in comparison to the overfilled assemblies.

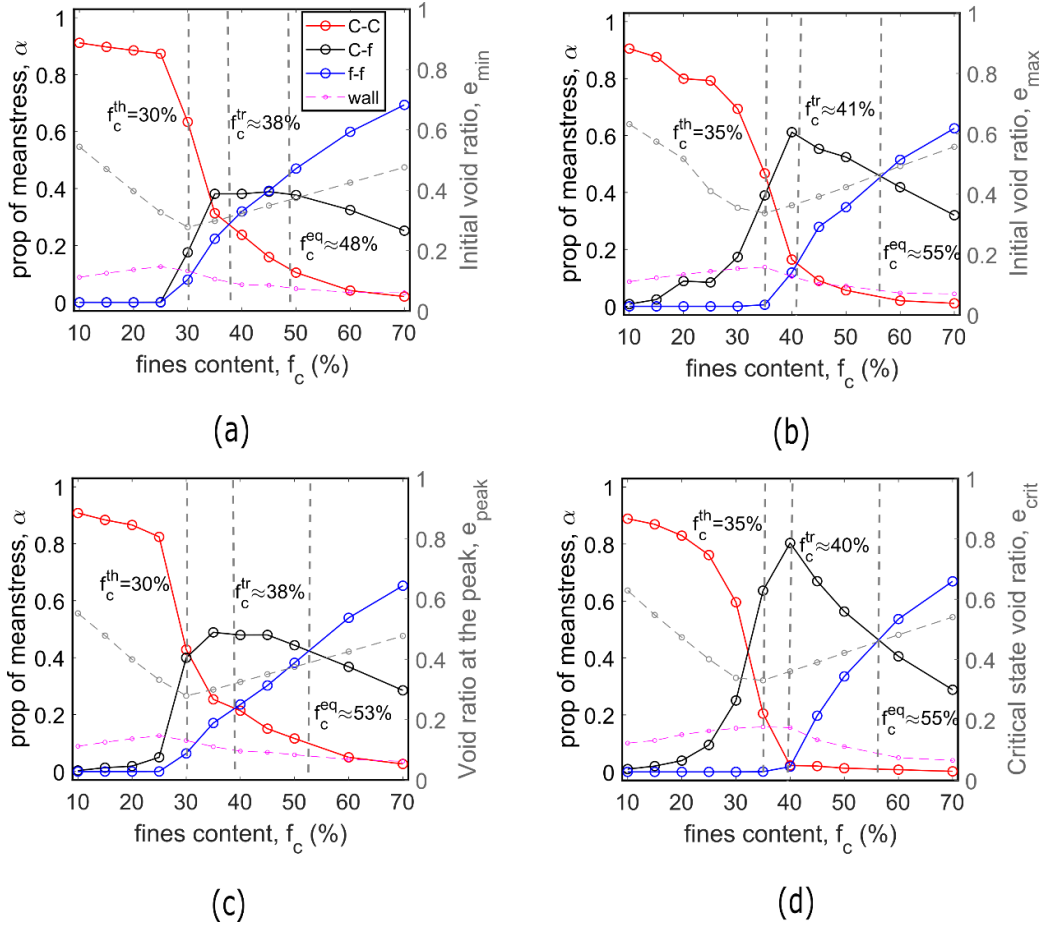


Fig. 16 Proportion of mean stress transmitted by contact type at (a) the initial state for dense assemblies b) the initial state for the loose assemblies (c) at the peak (d) the critical state (unique trends for both dense and loose assemblies). Void ratio data represented with dashed grey lines are plotted on the right side of each subplot to help identify the different regimes.

In a similar fashion to Fig. 11, Fig. 17 shows the proportion of all contacts belonging to each contact types at the different stages of shearing. The trends between the contact types here could be generally grouped into two categories delineated by the threshold fines content¹⁵.

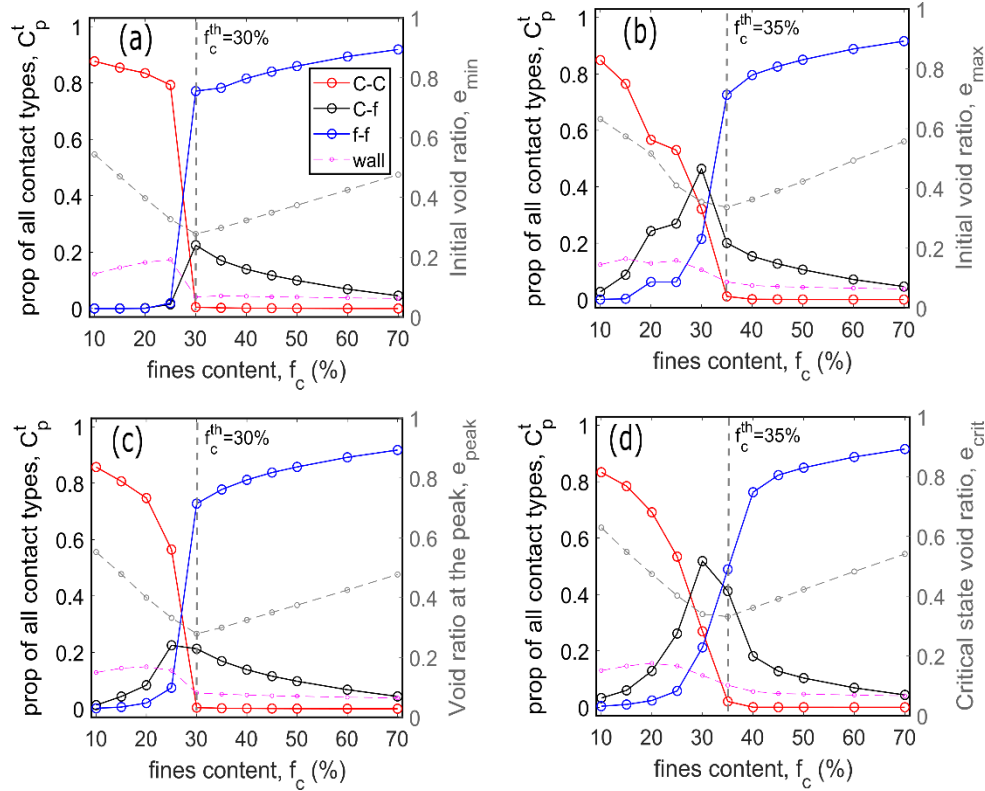
- For $f_c < f_c^{th}$, the proportions of the total contacts belonging to the f-f contacts, C_{f-f}^t , were lower than those belonging to the c-c contacts, C_{c-c}^t . The condition, $C_{c-c}^t > C_{c-f}^t > C_{f-f}^t$ generally holds, except for $f_c=30\%$ in the loose samples (Fig. 17b) and at the critical state (Fig. 17d) where the condition $C_{c-f}^t > C_{c-c}^t > C_{f-f}^t$ holds.
- For $f_c \geq f_c^{th}$, the f-f contacts dominate the assemblies, therefore the condition $C_{f-f}^t > C_{c-f}^t > C_{c-c}^t$ holds.

¹⁵ The proportions of all contact types belonging to the wall, C_{wl}^t were less than 0.17 and 0.08 for $f_c < f_c^{th}$ and for $f_c > f_c^{th}$, respectively.

536 From the threshold fines content, the C_{c-c}^t values were significantly low (ranging from 2.1×10^{-2}
537 $- 9 \times 10^{-5}$) at all states, and was zero for $f_c=70\%$ at the critical state (Fig. 17d). This show that the
538 fines disperse the coarse particles (i.e. C_{c-c}^t becomes minimal) from the threshold fines content,
539 f_c^{th} , which is in agreement with the 3D DEM study on binary mixtures by Minh et al., (2014),
540 and not beyond f_c^{th} as suggested in the experimental study on sandy-gravels by Skempton &
541 Brogan (1994). The suggestion by Salgado et al., (2000) in their experimental study, that the
542 fines controls the mechanical behaviour of sand-silt mixtures when the sand particles are
543 completely floating ($C_{c-c}^t \approx 0$) in the silts is not supported by the data shown here. While the
544 fines disperse the coarse particles from f_c^{th} , they did not become the primary stress-transmitting
545 matrix until f_c^{eq} is reached as explained in Section 4. In the transitional regime, there is the
546 possibility that some fines get trapped between the coarse particles while being loosely
547 connected to the rest of the fines in the assemblies.

548 Also, while for $f_c < f_c^{th}$, the $C_{c-f}^t \approx 0$ in the dense assemblies (Fig. 17a), in the loose assemblies
549 (Fig. 17b), $C_{c-f}^t > 0$. This suggests that, in agreement with Thevanayagam et al., (2002) and
550 Shire, (2014), the fines in the dense assemblies are confined within the voids between the
551 coarse particles with little interaction with the coarse matrix; in the loose assemblies, the fines
552 interact more with the coarse particles. The fact that the fines are interacting more with the
553 coarse particles in the loose case may indicate the fines are trapped within the coarse particles
554 thereby creating larger voids which may require more fines to fill in comparison to the dense
555 assemblies. This observation is consistent with Salgado et al., (2000) and Lade & Yamamuro
556 (1997) who found more fines on the surfaces of the coarse particles in their loose assemblies,
557 in comparison to the dense assemblies, and suggested that this is responsible for the larger drop
558 in the e_{min} than in the e_{max} for a given increase in the fines content. The drop in the e_{max} is
559 mitigated than in the e_{min} because the fines interacting with the coarse particles helps to create
560 larger voids hence the lower drop in the void ratio in the loose case.

561



562
 563 **Fig. 17** Proportion of the total contacts belonging to each category of contact type at (a) the
 564 initial state for dense assemblies (b) the initial state for the loose assemblies (c) the peak (d)
 565 the critical state (unique trends for both dense and loose assemblies). Void ratio data
 566 represented with dashed grey lines are plotted on the right side of each subplot to help identify
 567 the different regimes.

568
 569
 570
 571

6. Stress-based skeleton void ratio

572 The idea of sand skeleton void ratio was introduced in the experimental study by Kuerbis
 573 (1989) in order to understand the behaviour of silty sands with various fines content under
 574 undrained triaxial shearing. This proposition, which was based on a conceptual analysis of the
 575 fabric of soil mixtures, have been applied in other experimental and numerical studies
 576 (Benahmed et al., 2015; Chang & Yin, 2011; Lade & Yamamuro, 1997; Ni et al., 2004; Pitman
 577 et al., 1994; Rahman et al., 2008; Thevanayagam, 1998; Thevanayagam et al., 2002; Vaid,
 578 1994). In order to understand the critical state behaviour of the gap-graded assemblies
 579 subjected to drained shearing in this study, we propose a skeleton void ratio based on the stress
 580 sustained by individual particles. The skeleton void ratio, e_{skel} , is here defined as the void ratio
 581 of a granular system when the fines with particle stress, P^p , lower than a threshold stress value
 582 are regarded as part of the void space and are therefore excluded. Note that we propose to
 583 exclude only the fines (and not the coarse particles) for our skeleton void ratio calculation. This
 584 is based on the fact that loosely stressed fine particles may be eroded through the constrictions

585 of the soil matrix whereas coarse particles cannot as they are usually larger than the constriction
586 size (Garner & Fannin, 2010; ICOLD, 2017; A. W. Skempton & Brogan, 1994; Thevanayagam
587 & Mohan, 2000). In Figure 17 we show the variation of the proportion of the total mean stress
588 transmitted by the “skeleton” finer fraction, α_f^{skel} , for different stress thresholds, where the
589 threshold stress is defined as:

$$590 \quad \text{Threshold stress} = \underbrace{\alpha}_{\substack{\text{threshold} \\ \text{coefficient}}} \times \underbrace{\overline{P^p}}_{\substack{\text{Average} \\ \text{particle stress}}} \quad (10)$$

591 In Fig. 18, the threshold coefficient, α , ranges from 0 to 2.

- 592 - Unsurprisingly, the contribution of the fine remains negligible whatever the threshold
593 value for $f_c < f_c^{th}$ (the contribution for all the fines, α_f , is already negligible).
- 594 - For $f_c^{th} \leq f_c \leq 45\%$, generally no change is observed in α_f^{skel} until $\alpha = 0.1$, which
595 means that the fine grains transmitting a pressure P^p lower than 10% of the mean
596 pressure $\overline{P^p}$, contribute only marginally to the stress transmitted by the finer fraction.
- 597 - For $f_c > 45\%$, no change was observed in α_f^{skel} until $\alpha > 0.25$.

598 From the above analysis, we can retain $\alpha=0.1$ as a reasonable threshold to define the skeleton
599 fines for all fines content.

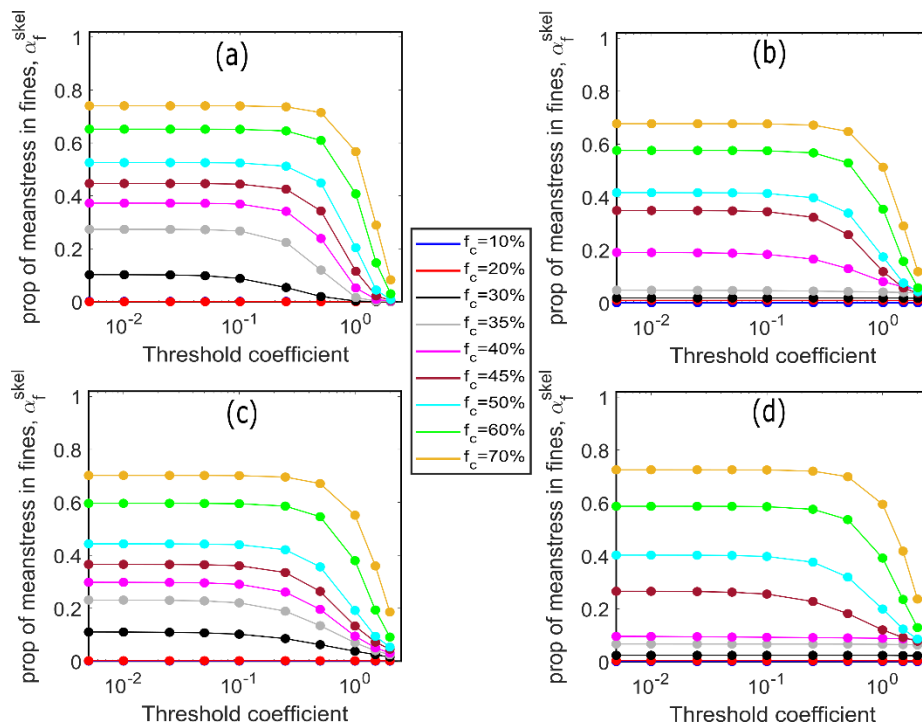
600 Fig. 19 shows the proportion of the fines left in an assembly after each exclusion. These
601 “skeleton” fines are included in the solid volume while computing the stress-based skeleton
602 void ratio, e_{skel} plotted in Fig. 20. For $f_c \geq f_c^{th}$, the proportion of the fines included as part of
603 the assembly skeleton decreases monotonically as the threshold stress increases (Fig. 19a-d).

604 The mechanical void ratio, e_{mech} has been computed in the literature as an alternative void
605 ratio index to the void ratio, e , of granular materials (Liu et al., 2022; Otsubo, 2016).
606 e_{mech} excludes the particles with $c \leq 1$. In Fig. 20, we compare the evolutions of e , e_{mech} and
607 e_{skel} (for $\alpha = 0.1$), $e_{skel}; \alpha = 0.1$, for the different fines contents. These evolutions are put in
608 parallel with the peak and the critical state stress ratios.

609 As shown in Figure 19, $e_{skel}; \alpha = 0.1$, shows a negative correlation with the critical state
610 strength, $(q/p)_{crit}$ (Fig. 20b & d), and no correlation with the peak strength, $(q/p)_{max}$ (Fig.
611 20a). Instead, at the peak, $(q/p)_{max}$ correlates negatively with e , (Fig. 20a & c), in agreement
612 with established relationship between the initial void ratio and the peak strength in the literature
613 (Adesina et al., 2023; Holubec & D’Appolonia, 1973; Ng, 2004). In order to determine the best
614 performing void ratio index among the indexes considered here, we estimated the goodness of
615 the fit, R^2 , for the relationship between the void ratio values determined using the indexes and
616 the strength exhibited by the assemblies (Table A.1 in the Appendix C). It is obvious that

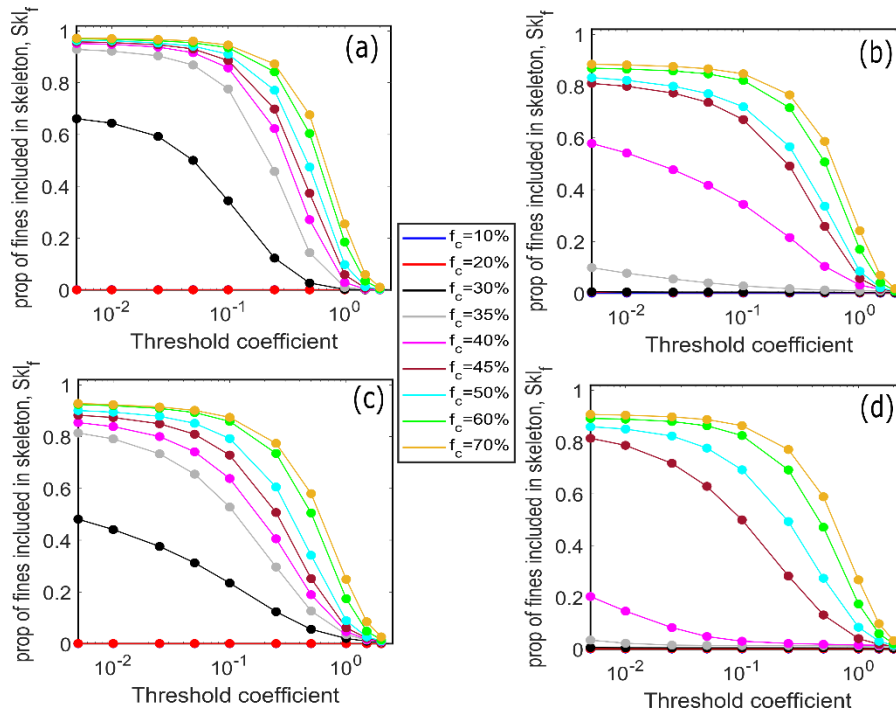
617 e_{skel} ; $x = 0.1$ provides the best fit ($R^2=0.84$) thereby yielding the best prediction of $(q/p)_{crit}$,
618 while the best performing void ratio index for $(q/p)_{max}$ is e ($R^2=0.90$ for underfilled and
619 $R^2=0.97$ for the overfilled assemblies). This finding is consistent with the fact that the
620 microstructure of granular assemblies (including the force chain network) evolve rapidly under
621 shearing at the critical state (Deng et al., 2022; Wautier et al., 2018). Consequently, the non-
622 active and the marginally active fines do not have the chance to interact with the force chains
623 and should therefore not be considered as part of the void when assessing the mechanical
624 behaviour. On the contrary, at the peak, although the non-active and the marginally active fines
625 do not contribute significantly to the total mean stress, they serve as a support for the force
626 chain network and as a result constitute an important part of the microstructure of the
627 assemblies (Tordesillas et al., 2010; Wautier et al., 2018; Zhu et al., 2016a; Zhu et al., 2016b).
628 Therefore, they have to be taken into account in the void ratio calculation.

629



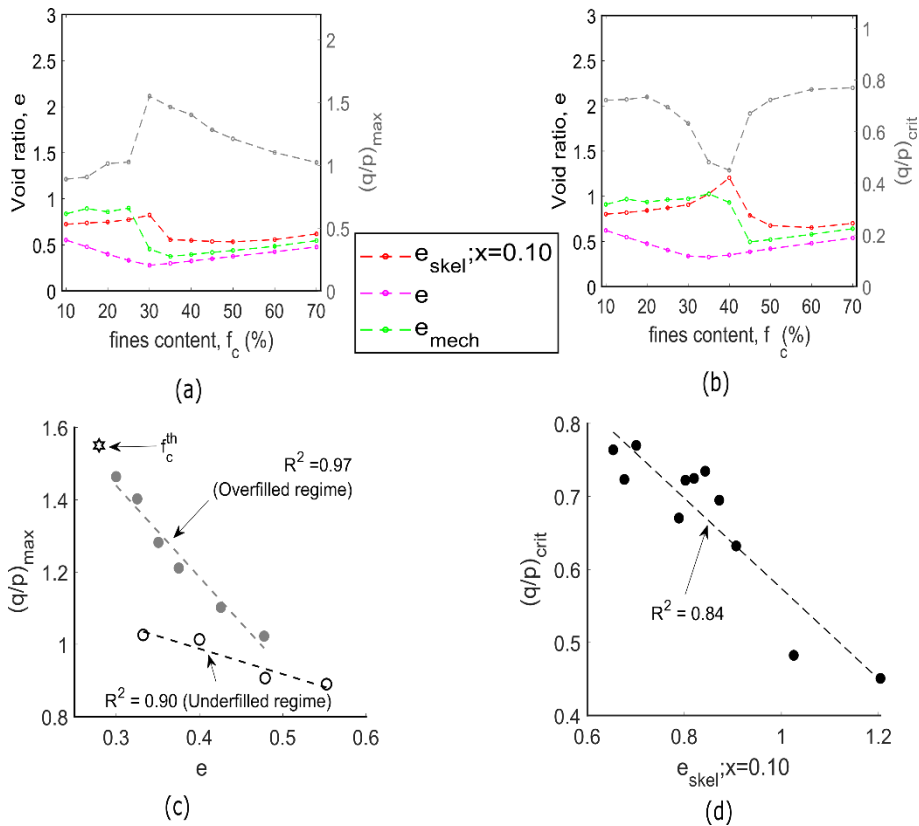
630

631 **Fig. 18** Estimation of the proportion of the mean stress transmitted by the finer fraction when
632 particles with particle stress lower than a threshold are excluded (a) dense; initial state (b) loose;
633 initial state (c) dense; peak state (d) critical state (unique trends for both dense and loose
634 assemblies)



635
 636 **Fig. 19** Proportion of skeleton fines as a function of the threshold coefficient (a) dense; initial
 637 state (b) loose; initial state (c) dense; peak state (d) critical state (unique trends for both dense
 638 and loose assemblies)

639
 640



641
 642 **Fig. 20** (a) void ratio indexes at the peak and $(q/p)_{max}$ (b) void ratio indexes at the critical
 643 state and $(q/p)_{crit}$, for different f_c values. Relationship between (c) e and $(q/p)_{max}$ (d)
 644 $e_{skel;x=0.1}$ and $(q/p)_{crit}$.

645

646 7. Summary and Conclusions

647 This study presents a micromechanical evaluation of the regimes delineating the behaviour of
648 gap-graded granular assemblies of different fines content, using discrete element simulations.
649 The existence of the regimes delineated by milestone fines content was assessed using the
650 macromechanical and micromechanical characteristics of the assemblies, and the contributions
651 of the particle size fractions and contact types to the total mean stress. The key findings and
652 conclusions are presented below.

- 653 (i) Two regimes were identified based on the macroscopic characteristics of the
654 assemblies, three regimes based on particle scale analysis and four regimes based
655 on contact scale analysis. We provide distinct delineations of the regimes by fines
656 content, in an original manner. Fig. 21 presents a summary of all the regimes
657 identified in this study. Table 3 highlights the unique trends characterising the three
658 regimes identified based on the macromechanical and the micromechanical
659 analyses conducted. We showed that the boundaries delineating the identified
660 regimes depend on density and stress state. We acknowledge that the boundaries
661 can also vary with a change in particle size ratio (and more generally a change in
662 coarse and fine particle size distributions) which is beyond the scope of our study.
- 663 (ii) The micromechanical analyses adopted overcome the limitation of experimental
664 studies where it is difficult to ascertain the claims emanating from the conceptual
665 analysis presented in the studies, since individual particles stresses or particle
666 dispersion cannot be easily determined in experiments. The claims that the fines
667 become the primary stress-transmitting matrix at the threshold fines content or at a
668 limiting fines content; or that stress is equally sheared by the coarse and the fine
669 particles in the transitional zone (Vallejo, 2001) or at $f_c > 35\%$ (Shire et al., 2014)
670 are not supported by the evidence provided here. Instead, we found that the coarse
671 particles are dispersed by the fines (i.e. where coarse to coarse contacts are minimal
672 or non-existent) from the threshold fines content. In addition, the fines do not
673 contribute to the total mean stress below the threshold fines content, they play a
674 secondary role in the transitional zone ($f_c \in [30\% ; 55\%]$ depending on density and
675 stress state), and only become the primary stress-transmitting matrix beyond the
676 transitional zone (i.e. when $f_c > f_c^{eq}$; $f_c^{eq} \in [48\% ; 55\%]$ depending on density and
677 stress state).

678 (iii) We found that the threshold stress which determines whether a fine particle
679 transmits a marginal or a significant stress with respect to the contribution of the
680 fines to the total mean stress is a fraction of the average particle stress, $\overline{P^p}$, within
681 an assembly; where the threshold stress values are $0.1 \times \overline{P^p}$ for $f_c^{th} \leq f_c \leq 45\%$, and
682 $0.25 \times \overline{P^p}$ for $f_c > 45\%$. The threshold stress concept proposed in this study can be
683 useful in determining the particles that constitute important mesostructures (i.e.
684 important force-chain networks) in gap-graded granular assemblies. The skeleton
685 void ratio determined based on the threshold stress correlates with the critical state
686 strength of the assemblies, while no correlation was found between the critical state
687 strength and alternative void ratio indexes such as the void ratio and the mechanical
688 void ratio at the critical state. The marginal stress transmitting fines (marginally
689 active fines) determined based on the threshold stress may constitute a part of the
690 particles susceptible to internal erosion, in addition to the non-inactive fines in a
691 gap-graded assembly (particles with zero or only one contact).

692 In addition to the standard underfilled and overfilled regimes, future DEM studies could focus
693 on the two transitional regimes identified here, and seek to understand the role played by
694 marginally active fines i) in the susceptibility of gap-graded assemblies to internal erosion and
695 ii) in the triggering of mechanical instabilities. As an additional perspective, the distinct
696 characteristics of the regimes shown in this study will prove useful in the development of
697 micromechanical models for gap-graded materials in which the typical mesoscale grain
698 arrangements can be tailored for each regime.

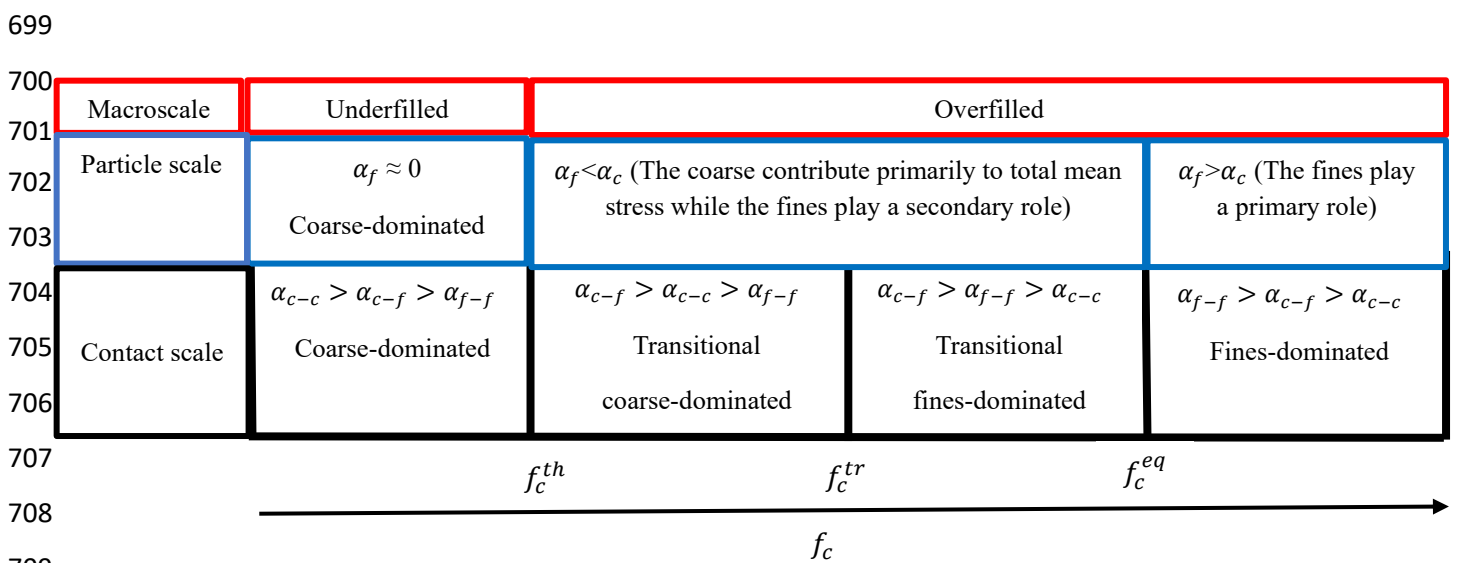


Fig. 21 Regime identification by macroscale, particle scale and contact scale characteristics

712 **Notations**

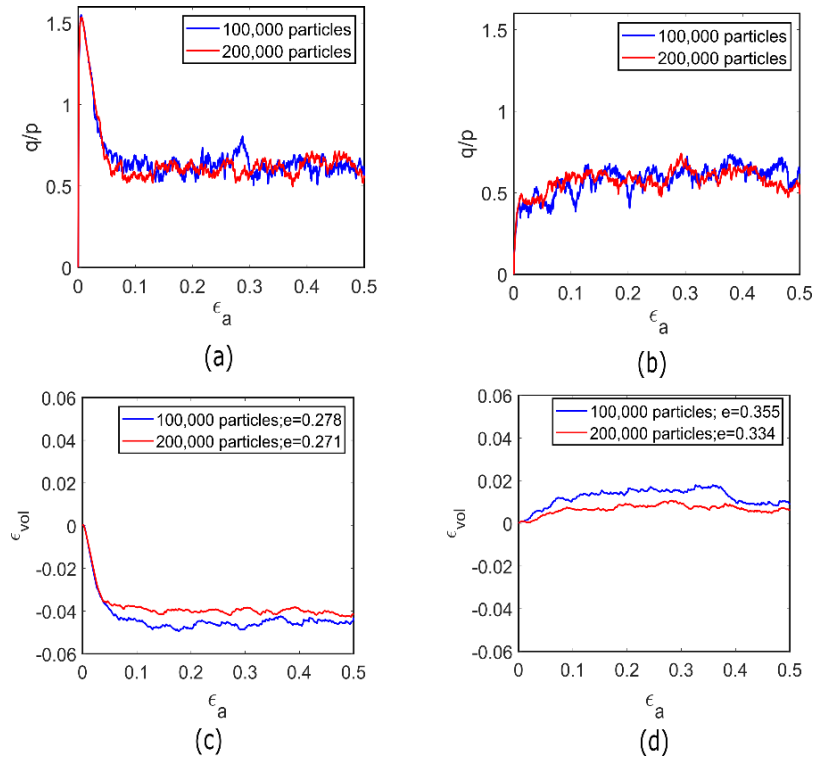
713	C	Total number of contacts in a granular system
714	C_{c-c}^t	The proportion of all contact types belonging to the c-c contacts
715	C_{c-f}^t	The proportion of all contact types belonging to the c-f contacts
716	C_{f-f}^t	The proportion of all contact types belonging to the f-f contacts
717	C_{wl}^t	The proportion of all contact types belonging to the wall
718	C_n^f	Proportion of the total number contacts belonging to the finer fraction
719	C_n^c	Proportion of the total number contacts belonging to the coarser fraction
720	d_{50}	Mean size of the fine grains
721	D_{50}	Mean size of the coarse grains
722	e_{max}	Maximum void ratio
723	e_{min}	Minimum void ratio
724	e_{crit}	Void ratio at the critical state
725	e_{hc}	Void ratio of the host sand
726	e_{hf}	Void ratio of the silt
727	ε_a	Axial strain (in y-direction)
728	ε_q	Deviatoric strain
729	ε_{vol}	Volumetric strain
730	f_c	Fines content
731	f_{th}	Threshold fines content
732	f_c^{th}	Threshold fines content
733	f_c^L	Limiting fines content
734	f_j^c	Contact force vector
735	l	Unit branch vector
736	N_p	Number of particles in the granular system
737	N_c	Number of contacts in a granular system
738	N_p^c	Number of coarse particles in the system
739	N_p^f	Number of fine particles in the system
740	N_c^p	Number of contacts involving a particle
741	N_0	Number of particles with no contact
742	N_1	Number of particles with one contact
743	$N_{c \geq 1}$	Number of coarse particles with one or more contacts
744	$N_{f \geq 1}$	Number of fine particles with one or more contacts
745	NC_f	Normalised total contacts for the coarser fraction
746	NC_f	Normalised total contacts for the finer fraction
747	n_i	Unit branch vector
748	p	Mean effective stress
749	p^c	Mean stress transmitted by the coarser fraction
750	p^f	Mean stress transmitted by the finer fraction
751	p^k	Mean stress transmitted by a contact type
752	P^p	Particle mean stress
753	$\overline{P^p}$	Average particle mean stress
754	α_c	Proportion of the total mean stress transmitted by the coarser fraction
755	α_f	Proportion of the total mean stress transmitted by the finer fraction
756	α_k	Proportion of the total mean stress transmitted a contact type
757	$(q/p)_{max}$	Stress ratio at the peak
758	$(q/p)_{crit}$	Stress ratio at the critical state

759	q	Deviatoric stress
760	q^f	Deviatoric stress transmitted by the finer fraction
761	q^c	Deviatoric stress transmitted by the coarser fraction
762	q_f	Proportion of the deviatoric stress transmitted by the finer fraction
763	R-squared	Goodness of fit
764	R_d	Ratio of the mean size of the coarse grains to the mean size of the fine grains
765	R_p	Radius of particle
766	R_1	Radius of first particle in contact
767	R_2	Radius of second particle in contact
768	R_f	Proportion of non-active fines
769	e_{skel}	Skeleton void ratio
770	$e_{skel;x}$	Skeleton void ratio determined using a threshold coefficient
771	SkI_f	Proportion of fines included in skeleton
772	x	Threshold coefficient
773	μ_{prep}	Inter-particle friction coefficient during assembly preparation (isotropic
774		compression)
775	μ	Inter-particle friction coefficient
776	λ	Size fraction
777	V	Volume of system
778	V^p	Volume of particle
779	σ_{zz}	Normal stress in z -direction
780	σ_{yy}	Normal stress in y -direction
781	σ_{xx}	Normal stress in x -direction
782	σ_{ij}	Second order stress tensor
783	σ_{ij}^c	Second order stress tensor for all contacts
784	σ_{ij}^p	Second order stress tensor for a particle
785	σ_p^c	Average mean stress transmitted by the coarser fraction
786	σ_p^f	Average mean stress transmitted by the finer fraction
787	ϕ	Friction angle
788	ϕ_p	Peak friction angle
789	ϕ_c	Critical state friction angle
790	ψ_{max}	Maximum dilatancy angle
791	Z	Mean coordination number
792	Z_{ini}	Mean coordination number at the initial state (after isotropic compression)
793	Z_{crit}	Mean coordination number at the critical state
794	Z_g	Geometrical coordination number
795	Z_{gc}	Geometrical coordination number for coarse particles
796	Z_{gf}	Geometrical coordination number for fine particles
797	Z_m	Mechanical coordination number
798	Z_{mc}	Mechanical coordination number for coarse particles
799	Z_{mf}	Mechanical coordination number for fine particles
800		
801		
802		
803		
804		
805		

806 **Appendix A. REV scale analysis**

807 In order to confirm that the sample size of 100,000 particles used for all f_c in this study is a
 808 representative element volume (REV), in Fig. A.1, we show that increasing the assembly size
 809 to 200,000 particles for both the dense and loose assemblies having $f_c = 30\%$ did not
 810 significantly influence the stress-strain responses. The slight sensitivity to assembly size
 811 observed in the volumetric strains was also reported in the DEM study on REV for granular
 812 materials by Adesina et al., (2022) and can be attributed to the small variation in the initial void
 813 ratio of the assemblies. The REV test is shown here for $f_c = 30\%$ because it represents the
 814 threshold fines content and is the fines content with the highest coarse-fine particle interaction
 815 (Fig. 17) which indicates the largest REV size.

816



817

818 **Fig. A.1** Effect of assembly size on (i) the stress-strain responses for dense assemblies
 819 ($\mu_{prep}=0.03$) and (ii) loose assemblies ($\mu_{prep}=0.5$) (iii) volumetric strain responses for the
 820 dense assemblies and (iv) the loose assemblies having $f_c = 30\%$

821

822

823

824

825

826

827

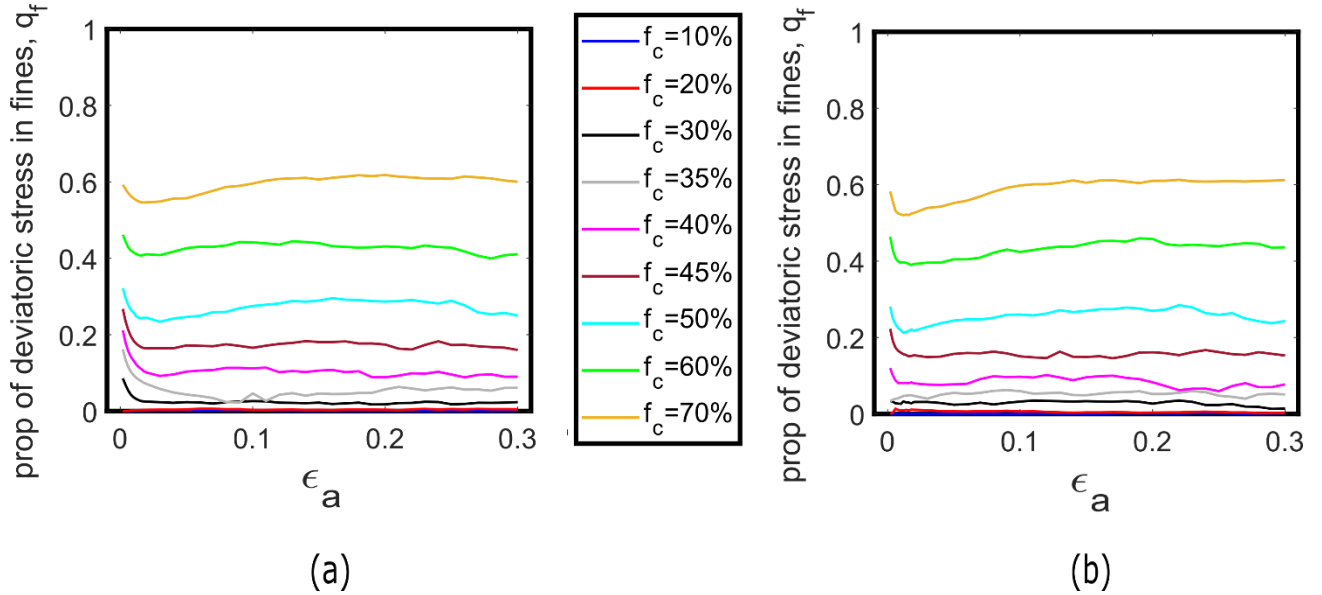
828 **Appendix B. Fine contribution to deviatoric stress**

829 Fig. A.2 shows the evolution of the proportion of the deviatoric stress, q , transmitted by the
 830 fines during shearing, for dense and loose assemblies of different fines content, f_c . Provided
 831 that all stress tensors are diagonal in the frame (x, y, z) , the deviatoric stress for the entire
 832 system is calculated as:

$$833 \quad q = \sigma_{zz} - (\sigma_{xx} + \sigma_{yy})/2 \quad (A1)$$

834 Similar to the mean stress (see Section 4), the proportion of the total deviatoric stress
 835 transmitted by the finer fraction, q_f , is calculated as q^f/q , while the proportion of the total
 836 deviatoric stress transmitted by the coarser fraction, q_c , is calculated as q^c/q , where q^f and
 837 q^c are the deviatoric stress transmitted by the finer and the coarser populations, respectively.

838 As expected, the q_f data is generally similar to the α_f data presented in Fig. 9. It is worthy of
 839 note that the q_f data presented in Fig. A2 starts after the initial state, at $\epsilon_a = 0.02$, since $q = 0$
 840 at the initial state. We observed that for $f_c \geq 30\%$, the magnitude of q_f is lower than the
 841 magnitude of α_f during shearing. This indicates that the stress is more isotropic in the finer
 842 fraction than in the coarser fraction.



843 (a) 844 **Fig. A.2** Evolution of the proportion of deviatoric stress transmitted by the fines during
 845 shearing for (a) dense assemblies (b) loose assemblies

846
847
848
849

850

851 **Appendix C. Sensitivity analysis to the threshold coefficient used in the definition of the**
 852 **skeleton void ratio.**

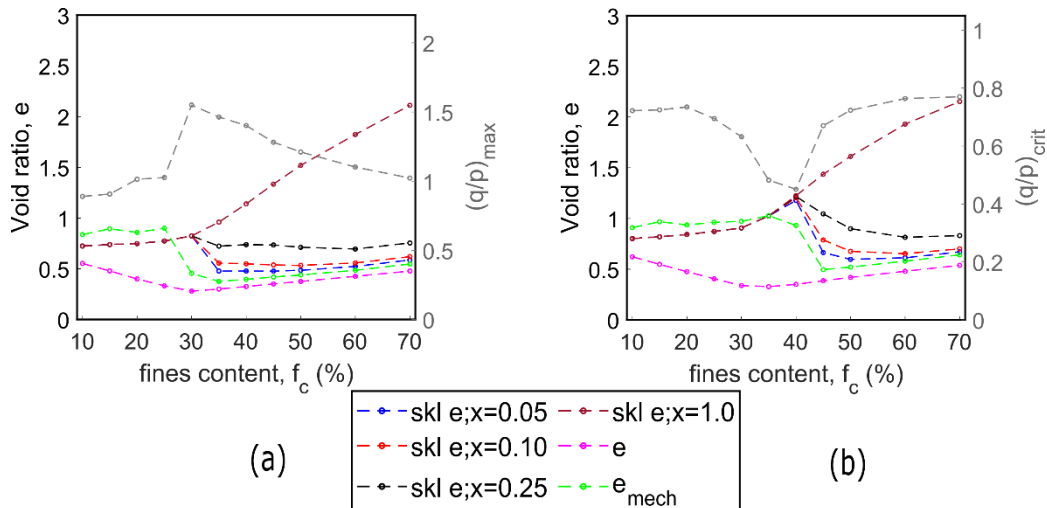
853 In Table A.1 and Fig. A.3, we show that at the critical state, $e_{skel}; x = 0.1$ exhibited a negative
 854 correlation with $(q/p)_{crit}$ and yielded the highest R-squared value ($R^2=0.84$), while both the
 855 e and e_{mech} do not correlate with $(q/p)_{crit}$. $e_{skel}; x = 0.05$ and $e_{skel}; x = 0.25$ also yielded a
 856 negative correlation with $(q/p)_{crit}$, with $R^2=0.73$ and $R^2=0.76$, respectively. $e_{skel}; x = 1$
 857 yielded a poor correlation ($R^2=0.08$) with $(q/p)_{crit}$, indicating that using a threshold
 858 coefficient, $x = 1$, for the skeleton void ratio calculation for the gap-graded assemblies,
 859 resulted in the exclusion of important stress-transmitting fines, especially from the overfilled
 860 assemblies. $x = 1$ is the standard for defining force-chains for narrowly-graded assemblies
 861 (Peters et al., 2005). In agreement with earlier studies (Adesina et al., 2023; Holubec &
 862 D'Appolonia, 1973; Ng, 2004), at the peak, e , correlates negatively with $(q/p)_{max}$, and
 863 yielded the highest R-squared value ($R^2=0.97$), followed by e_{mech} ($R^2=0.66$). e_{skel} correlated
 864 poorly with $(q/p)_{max}$.

865

866 **Table A.1** Assessment of void ratio indexes with the strength value, (q/p)

Void ratio index	e	e_{mech}	$e_{skel}; x=0.05$	$e_{skel}; x=0.10$	$e_{skel}; x=0.25$	$e_{skel}; x=1.0$
R^2_{peak}	0.965	0.656	0.119	0.074	-	9.55e-5
R^2_{crit}	-	0.208	0.725	0.844	0.764	0.08

867 Note: The R^2 values here are determined from inverse relationship between strength and void ratio. ‘-’ means
 868 strength increased with void ratio as against established relationship between strength and void ratio.
 869



870

871 **Fig. A.3** Relationship between (a) void ratio indexes and peak q/p , $(q/p)_{max}$ (b) void ratio
 872 indexes and critical state q/p , $(q/p)_{crit}$

873

874

875 **Acknowledgement**

876 This work was supported by the National Research Agency (ANR), France. It is a product of
877 the research project titled “Micro-scale driven Models for Discrete for Discrete Materials
878 (MiMoDiM)”, with the reference, ANR-22-CE46-0001. A CC-BY public copyright license has
879 been applied by the authors to the present document and will be applied to all subsequent
880 versions up to the Author Accepted Manuscript arising from this submission, in accordance
881 with the grant’s open access conditions.

882

883 **Credit Authorship**

884 **Peter Adesina:** Conceptualization, Methodology, Investigation, Formal analysis,
885 Visualization, Writing – original draft.

886 **Antoine Wautier:** Funding acquisition, Conceptualization, Methodology, Supervision,
887 Writing – review & editing.

888 **Nadia Benahmed:** Conceptualization, Methodology, Supervision, Writing – review &
889 editing.

890

891 **Compliance with ethical standards**

892 **Conflict of interest** The authors declare that there is no conflict of interests regarding the
893 publication of this article. Publication has been approved by all authors. None of the material
894 presented in the paper is submitted or published elsewhere.

895

896

897 **References**

898

899 Adesina, P. A., O’Sullivan, C., & Wang, T. (2023). DEM study on the effect of particle shape
900 on the shear behaviour of granular materials. *Computational Particle Mechanics*,
901 *Accepted*.

902 Adesina, P., O’Sullivan, C., Morimoto, T., & Otsubo, M. (2022). Determining a
903 representative element volume for DEM simulations of samples with non-circular
904 particles. *Particuology*, *68*, 29–43. <https://doi.org/10.1016/j.partic.2021.10.007>

905 Adesina, P., O’Sullivan, C., & Wang, T. (2024). Understanding the interplay between particle
906 shape, grading and sample density on the behaviour of granular assemblies: A DEM
907 approach. *Granular Matter*, *26*(1). <https://doi.org/10.1007/s10035-023-01383-2>

908 Bagi, K. (1999). Microstructural stress tensor of granular assemblies with volume forces.
909 *Journal of Applied Mechanics, Transactions ASME*, *66*(4), 934–936.
910 <https://doi.org/10.1115/1.2791800>

911 Benahmed, N., Nguyen, T. K., Hicher, P. Y., & Nicolas, M. (2015). An experimental
912 investigation into the effects of low plastic fines content on the behaviour of sand/silt
913 mixtures. *European Journal of Environmental and Civil Engineering*, *19*(1), 109–128.
914 <https://doi.org/10.1080/19648189.2014.939304>

915 Bolton, M. D. (1986). The strength and dilatancy of sands. *Geotechnique*, *36*(1), 65–78.

916 Chang, C. S., & Yin, Z. Y. (2011). Micromechanical modeling for behavior of silty sand with

917 influence of fine content. *International Journal of Solids and Structures*, 48(19), 2655–
918 2667. <https://doi.org/10.1016/j.ijsolstr.2011.05.014>

919 Cubrinovski, M., & Ishihara, K. (2002). Maximum and minimum void ratio characteristics of
920 sands. *Soils and Foundations*, 42(6), 65–78. https://doi.org/10.3208/sandf.42.6_65

921 Cundall, P. A., & Strack, O. D. L. (1979). A discrete numerical model for granular
922 assemblies. *Geotechnique*, 30(3), 331–336. <https://doi.org/10.1680/geot.1980.30.3.331>

923 da Cruz, F., Emam, S., Prochnow, M., Roux, J., & Chevoir, F. (2005). Rheophysics of dense
924 granular materials : Discrete simulation of plane shear flows. *PHYSICAL REVIEW*,
925 72(February), 1–17. <https://doi.org/10.1103/PhysRevE.72.021309>

926 Deng, N., Wautier, A., Tordesillas, A., Thiery, Y., Yin, Z. Y., Hicher, P. Y., & Nicot, F.
927 (2022). Lifespan dynamics of cluster conformations in stationary regimes in granular
928 materials. *Physical Review E*, 105(1), 1–15.
929 <https://doi.org/10.1103/PhysRevE.105.014902>

930 Evans, D. M., & Zhou, S. (1995). Liquefaction Behaviour of Sand-Gravel Composites.
931 *Journal of Geotechnical and Geoenvironmental Engineering*, 121(3), 287–298.

932 Garner, S. J., & Fannin, R. J. (2010). Understanding internal erosion: a decade of research
933 following a sinkhole event. *International Journal on Hydropower and Dams*, 17(3), 93–
934 98.

935 Holubec, I., & D'Appolonia, E. (1973). Effect of particle shape on the Engineering Properties
936 of Granular Soils. *Evaluation of Relative Density and Its Role in Geotechnical Projects*
937 *Involving Cohesionless Soils, ASTM STP 523*, 304–318.
938 <https://doi.org/10.1051/epjconf/201714006006>

939 ICOLD. (2013). *Internal Erosion of Existing Dams, Levees and Dykes, and Their*
940 *Foundations. In: Bridle, R. and Fell, R., Eds., Bulletin 164, Volume 1: Internal Erosion*
941 *Processes and Engineering Assessment, International Commission on Large Dams,*
942 *Paris.*

943 ICOLD, I. C. on L. dams. (2017). *ICOLD Bulletin 164 on Internal erosion of existing dams,*
944 *levees and dikes, and their foundations.*

945 Jiang, M. D., Yang, Z. X., Barreto, D., & Xie, Y. H. (2018). The influence of particle-size
946 distribution on critical state behavior of spherical and non-spherical particle assemblies.
947 *Granular Matter*, 20(4), 1–15. <https://doi.org/10.1007/s10035-018-0850-x>

948 Kuerbis, R. H. (1989). Effect of gradation and fines content on the undrained response of
949 sand. In *Department of Civil Engineering, The University of British Columbia.*
950 [https://doi.org/10.1016/0148-9062\(90\)90054-6](https://doi.org/10.1016/0148-9062(90)90054-6)

951 Lade, P. V., Liggió, C. D., & Yamamuro, J. A. (1998). Effects of Non-Plastic Fines on
952 Minimum and Maximum Void Ratios of Sand. *Geotechnical Testing Journal*, 21(4),
953 336–347. <https://doi.org/10.1520/gtj11373j>

954 Lade, P. V., & Yamamuro, J. A. (1997). Effects of nonplastic fines on static liquefaction of
955 sands. *Canadian Geotechnical Journal*, 34(6), 918–928. <https://doi.org/10.1139/t97-052>

956 Li, W., Chu, Y., Deng, G., Cai, H., Xie, D., & Lee Lee, M. (2023). Study of shear induced
957 stress redistribution in gap-graded soils by discrete element method. *Computers and*
958 *Geotechnics*, 156(June 2022), 105248. <https://doi.org/10.1016/j.compgeo.2023.105248>

959 Li, Y., Otsubo, M., Ghaemi, A., Dutta, T. T., & Kuwano, R. (2022). Transition of gap-graded
960 soil fabric – shear wave measurements and dispersion relation. *Soils and Foundations*,
961 62(1), 101092. <https://doi.org/10.1016/j.sandf.2021.101092>

962 Liu, D., Morimoto, T., Carraro, J. A. H., & O'Sullivan, C. (2022). A semi-empirical re-
963 evaluation of the influence of state on elastic stiffness in granular materials. *Granular*
964 *Matter*, 24(2). <https://doi.org/10.1007/s10035-022-01215-9>

965 Minh, N. H., Cheng, Y. P., & Thornton, C. (2014). Strong force networks in granular
966 mixtures. *Granular Matter*, 16(1), 69–78. <https://doi.org/10.1007/s10035-013-0455-3>

967 Ng, T.-T. (2004). Triaxial Test Simulations with Discrete Element Method and Hydrostatic
968 Boundaries. *Journal of Engineering Mechanics*, 130(10), 1188–1194.
969 [https://doi.org/10.1061/\(asce\)0733-9399\(2004\)130:10\(1188\)](https://doi.org/10.1061/(asce)0733-9399(2004)130:10(1188))

970 Ni, Q., Tan, T. S., Dasari, G. R., & Hight, D. W. (2004). Contribution of fines to the
971 compressive strength of mixed soils. *Geotechnique*, 54(9), 561–569.
972 <https://doi.org/10.1680/geot.2004.54.9.561>

973 Nicot, F., Hadda, N., Guessasma, M., Fortin, J., & Millet, O. (2013). On the definition of the
974 stress tensor in granular media. *International Journal of Solids and Structures*, 50(14–
975 15), 2508–2517. <https://doi.org/10.1016/j.ijsolstr.2013.04.001>

976 Otsubo, M. (2016). *Particle Scale Analysis of Soil Stiffness and Elastic Wave Propagation*.

977 Peters, J. F., Muthuswamy, M., Wibowo, J., & Tordesillas, A. (2005). Characterization of
978 force chains in granular material. *Physical Review E - Statistical, Nonlinear, and Soft
979 Matter Physics*, 72(4), 1–8. <https://doi.org/10.1103/PhysRevE.72.041307>

980 Pitman, T. D., Robertson, P. K., & Segoo, D. C. (1994). Influence of fines on the collapse of
981 loose sands. *Canadian Geotechnical Journal*, 31(5), 728–739.
982 <https://doi.org/10.1139/t94-084>

983 Rahman, M. M., Lo, S. R., & Gnanendran, C. T. (2008). On equivalent granular void ratio
984 and steady state behaviour of loose sand with fines. *Canadian Geotechnical Journal*,
985 45(10), 1439–1456. <https://doi.org/10.1139/T08-064>

986 Salgado, R., Bandini, P., & Karim, A. (2000). Shear Strength and Stiffness of Silty Sand.
987 *Journal of Geotechnical and Geoenvironmental Engineering*, 126(5), 451–462.

988 Sarkar, D., Goudarzy, M., König, D., & Wichtmann, T. (2020). Influence of particle shape
989 and size on the threshold fines content and the limit index void ratios of sands
990 containing non-plastic fines. *Soils and Foundations*, 60(3), 621–633.
991 <https://doi.org/10.1016/j.sandf.2020.02.006>

992 Shire, T. (2014). *Micro-scale Modelling of Granular Filters. Thesis submitted to the
993 Department of Civil and Engineering Civil and Environmental Engineering, Imperial
994 College, London, United Kingdom*.

995 Shire, T., O’Sullivan, C., & Hanley, K. J. (2016). The influence of fines content and size-
996 ratio on the micro-scale properties of dense bimodal materials. *Granular Matter*, 18(3).
997 <https://doi.org/10.1007/s10035-016-0654-9>

998 Shire, T., O’Sullivan, C., Hanley, K. J., & Fannin, R. J. (2014). Fabric and Effective Stress
999 Distribution in Internally Unstable Soils. *Journal of Geotechnical and
1000 Geoenvironmental Engineering*, 140(12), 04014072.
1001 [https://doi.org/10.1061/\(ASCE\)GT.1943-5606.0001184](https://doi.org/10.1061/(ASCE)GT.1943-5606.0001184)

1002 Skempton, A., & Brogan, J. (1994). Experiments on piping in sandy gravels. *Géotechnique*,
1003 44(3), 449–460.

1004 Skempton, A. W., & Brogan, J. M. (1994). Experiments on piping in sandy gravels.
1005 *Geotechnique*, 44(3), 449–460. <https://doi.org/10.1680/geot.1995.45.3.565>

1006 Šmilauer et al, V. (2021). *Yade Documentation 3rd ed. The Yade Project* (p.
1007 DOI:10.5281/zenodo.5705394 (<http://yade-dem.org/do>)).

1008 Sufian, A., Artigaut, M., Shire, T., & O’Sullivan, C. (2021). Influence of Fabric on Stress
1009 Distribution in Gap-Graded Soil. *Journal of Geotechnical and Geoenvironmental
1010 Engineering*, 147(5), 1–14. [https://doi.org/10.1061/\(asce\)gt.1943-5606.0002487](https://doi.org/10.1061/(asce)gt.1943-5606.0002487)

1011 Thevanayagam, S. (1998). Effect of Fines and Confining Stress on Undrained Shear Strength
1012 of Silty Sands. *Journal of Geotechnical and Geoenvironmental Engineering*, 124(6),
1013 479–491. [https://doi.org/10.1061/\(asce\)1090-0241\(1999\)125:11\(1024\)](https://doi.org/10.1061/(asce)1090-0241(1999)125:11(1024))

1014 Thevanayagam, S., & Mohan, S. (2000). Intergranular state variables and stress-strain
1015 behaviour of silty sands. *Geotechnique*, 50(1), 1–23.
1016 <https://doi.org/10.1680/geot.2000.50.1.1>

- 1017 Thevanayagam, S., Shenthnan, T., Mohan, S., & Liang, J. (2002). Undrained Fragility of
 1018 Clean Sands, Silty Sands, and Sandy Silts. *Journal of Geotechnical and*
 1019 *Geoenvironmental Engineering*, 128(10), 849–859. [https://doi.org/10.1061/\(asce\)1090-](https://doi.org/10.1061/(asce)1090-)
 1020 0241(2002)128:10(849)
- 1021 Thornton, C. (2000). Numerical simulations of deviatoric shear deformation of granular
 1022 media. *Geotechnique*, 50(1), 43–53. <https://doi.org/10.1680/geot.2000.50.1.43>
- 1023 Thornton, C., & Anthony, S. J. (1998). Quasi-static deformation of particulate media. *Phil.*
 1024 *Trans. R. Soc. Lond. A*, 356, 2763–2782.
- 1025 Thornton, Colin. (2015). Granular Dynamics, Contact Mechanics and Particle System
 1026 Simulations: A DEM study. *Granular Dynamics, Contact Mechanics and Particle*
 1027 *System Simulations: A DEM Study*, 24, 1–195. [https://doi.org/10.1007/978-3-319-18711-](https://doi.org/10.1007/978-3-319-18711-2)
 1028 2
- 1029 Tordesillas, A., Walker, D. M., & Lin, Q. (2010). Force cycles and force chains. *Physical*
 1030 *Review E - Statistical, Nonlinear, and Soft Matter Physics*, 81(1), 5–7.
 1031 <https://doi.org/10.1103/PhysRevE.81.011302>
- 1032 Vaid, Y. P. (1994). Liquefaction of silty soils. In: *Proceedings of Ground Failures Under*
 1033 *Seismic Conditions. Geotech. Spec. Publ. 44, ASCE, New York*, 1–16.
- 1034 Vaid, Y. P., & Sasitharan, S. (1992). The strength and dilatancy of sand. *Canadian*
 1035 *Geotechnical Journal*, 29, 522–526. <https://doi.org/10.1680/geot.1987.37.4.517>
- 1036 Vallejo, L. E. (2001). Interpretation of the limits in shear strength in binary granular
 1037 mixtures. *Canadian Geotechnical Journal*, 38(5), 1097–1104.
 1038 <https://doi.org/10.1139/cgj-38-5-1097>
- 1039 Wang, T., Liu, S., Wautier, A., & Nicot, F. (2022). Updated skeleton void ratio for gravelly
 1040 sand mixtures considering the effect of grain size distribution. *Canadian Geotechnical*
 1041 *Journal*, 59(11), 12–23. <https://doi.org/10.1139/cgj-2021-0443>
- 1042 Wautier, A., Bonelli, S., & Nicot, F. (2018). Micro-inertia origin of instabilities in granular
 1043 materials. *International Journal for Numerical and Analytical Methods in*
 1044 *Geomechanics*, 42(9), 1037–1056. <https://doi.org/10.1002/nag.2777>
- 1045 Xiao, Y., Xiang, J., Liu, H., & Ma, Q. (2017). Strength–dilatancy relation of sand containing
 1046 non-plastic fines. *Geotechnique Letters*, 7(2), 204–210.
 1047 <https://doi.org/10.1680/jgele.16.00144>
- 1048 Yang, S., Lacasse, S., & Sandven, R. (2005). Determination of the Transitional Fines Content
 1049 of Mixtures of Sand and Non-plastic Fines. *Geotechnical Testing Journal*, 29(2), 102–
 1050 107. <https://doi.org/10.1520/GTJ14010>
- 1051 Yin, Z. Y., Zhao, J., & Hicher, P. Y. (2014). A micromechanics-based model for sand-silt
 1052 mixtures. *International Journal of Solids and Structures*, 51(6), 1350–1363.
 1053 <https://doi.org/10.1016/j.ijsolstr.2013.12.027>
- 1054 Zhu, H., Nguyen, H. N. G., Nicot, F., & Darve, F. (2016). On a common critical state in
 1055 localized and diffuse failure modes. *Journal of the Mechanics and Physics of Solids*, 95,
 1056 112–131. <https://doi.org/10.1016/j.jmps.2016.05.026>
- 1057 Zhu, H., Nicot, F., & Darve, F. (2016). Meso-structure organization in two-dimensional
 1058 granular materials along biaxial loading path. *International Journal of Solids and*
 1059 *Structures*, 96, 25–37. <https://doi.org/10.1016/j.ijsolstr.2016.06.025>
- 1060 Zuo, L., & Baudet, B. A. (2015). Determination of the transitional fines content of sand-non
 1061 plastic fines mixtures. *Soils and Foundations*, 55(1), 213–219.
 1062 <https://doi.org/10.1016/j.sandf.2014.12.017>
- 1063
 1064
 1065